

INSTITUTE OF ELECTRONIC MATERIALS TECHNOLOGY

**MATERIAŁY
ELEKTRONICZNE
ELECTRONIC MATERIALS**

QUARTERLY

**Vol. 45, No. 1
2017**



Ministry of Science
and Higher Education
Republic of Poland

*Creating the English language version of the journal „Electronic Materials”
and digitalization of „Electronic Materials” to provide and maintain
open access through the Internet -
tasks financed in accordance with the 593/P-DUN/2017 agreement
from the funds of the Ministry of Science and Higher Education
intendend for the science dissemination.*

WARSAW ITME 2017

CONTENTS **4** Effect of Ti and Zr additions on wettability and work of adhesion in Ag/C system

Wettability in the silver/carbon system was examined by the sessile drop method under vacuum at the temperature of 1243 K. Vitreous carbon, diamond and graphite were used as solid substrates. After wettability tests, the solidified Ag/C and Ag-X/C (X - 1 wt.% Ti or Zr) couples were subjected to structural characterization by SEM and EDX analysis. Liquid pure silver does not wet these substrates and shows weak adhesion, regardless of the type of the carbon material used. The introduction of 1 wt.% carbide forming additions Ti or Zr into silver changes dramatically the interaction in the Ag/C system leading to the formation of continuous reaction product layers (TiC_x and ZrC_x , respectively) at the drop/substrate interface. These interfacial layers are responsible for good wetting and high work of adhesion between AgTi1 and AgZr1 alloys and all types of carbon materials examined in this study.

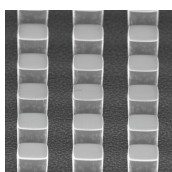
D. Wójcik-Grzybek,
K. Frydman,
N. Sobczak,
R. Nowak,
A. Piątkowska,
K. Pietrzak



12 The use of thermal mapping in evaluation of mechanically induced electrical degradation of graphene - based transparent heaters

The purpose of this study is to investigate temperature distributions of graphene-based transparent heaters deposited on glass. Furthermore it analyses the influence of layer discontinuities such as scratches and cracks on the performance of Joule-heated samples. Graphene mechanical strength was examined by the nanoscratch method at incremental loads using a ball on a flat sample surface. In the case of the controlled load several scratches were produced on the graphene surface. Tribological tests were conducted at different constant loads. The paper presents scanning electron micrograph (SEM) observations of the modified graphene surface. Infrared imaging of Joule-heated samples indicates a significant uniformity deterioration of the thermal maps due to the current flow alteration in the presence of structural imperfections. The results obtained in the course of this study give new insight into the role of defects such as cracks or discontinuities in the overall performance of graphene transparent layers.

A. Kozłowska,
G. Gawlik,
A. Piątkowska,
A. Krajewska,
W. Kaszub



18 Evaluation of hydrophobic properties of organic layers modified with graphene flakes

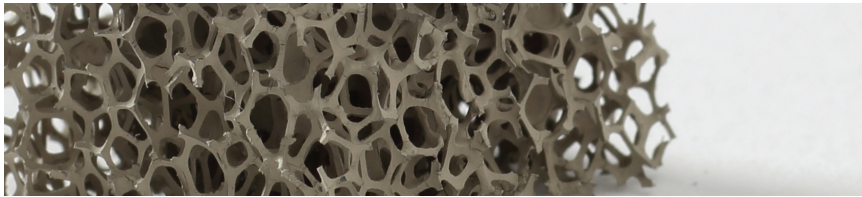
The paper presents the results of our research on graphene composites with organic polymers in various media. The following composites have been tested: PVDF/DMF/GR, PVDF/NMP/GR, PVDF/acetone/toluene/GR and PMMA/GR. The main purpose of this study is to evaluate hydrophobic properties of the selected materials by the contact measurements angle using the static method. The highest obtained value of the contact angle approached 180° for a superhydrophobic composite PVDF/acetone/toluene/GR.

B. Stańczyk,
K. Góra,
K. Jach,
L. Dobrzański

**On the cover:**

Ceramic foams made from silicon carbide and polyurethane matrix used to their production. Application: filters, catalyst carriers, ceramic-metal composites component

Sample from dr Katarzyna Jach.

**EDITORIAL OFFICE ADDRESS****Institute of Electronic Materials Technology**

Wólczyńska Str. 133, 01-919 Warsaw

e-mail: ointe@itme.edu.pl

[www: matelektron.itme.edu.pl](http://www:matelektron.itme.edu.pl)

EDITORIAL BOARD**Editor in Chief**

dr hab. inż. Katarzyna PIETRZAK, prof. ITME

Associate Editor

dr hab. inż. Paweł KAMIŃSKI, prof. ITME

Subject Editor:

dr inż. Marcin CHMIELEWSKI

dr inż. Tymoteusz CIUK

dr inż. Ewa DUMISZEWSKA

dr inż. Anna KOZŁOWSKA

Advisory Board:

prof. dr hab. Jacek BARANOWSKI

prof. dr hab. inż. Andrzej JELEŃSKI

dr hab. inż. Rafał KASZTELANIC, prof. ITME

dr hab. inż. Ludwika LIPIŃSKA, prof. ITME

prof. dr hab. Anna PAJĄCZKOWSKA

prof. dr hab. Ewa TALIK

prof. dr hab. inż. Andrzej TUROS

Advisory Assistant:

mgr Anna WAGA

Linguistic Editors:

mgr Maria SIWIK - GRUŻEWSKA

dr Mariusz ŁUKASZEWSKI

Technical Editor:

mgr Szymon PLASOTA

CONTACT

Editor in Chief phone: (22) 639 58 85

Editorial Assistant phone: (22) 639 55 29

PL ISSN 0209 - 0058

A quarterly quoted on the list of scientific journals of the Ministry of Science and Higher Education

7 points - according to the statement of the Ministry of Science and Higher Education.

Published articles are indexed in databases:

BazTech, CAS - Chemical Abstracts and Index Copernicus

Published articles of a scientific nature are reviewed by independent researchers.

The paper version is the primary version.

The quarterly is published in open access.

Circulation: 200 copies

Effect of Ti and Zr additions on wettability and work of adhesion in Ag/C system

Danuta Wójcik-Grzybek¹, Krystyna Frydman¹, Natalia Sobczak², Rafał Nowak², Anna Piątkowska¹, Katarzyna Pietrzak¹

Wettability in the silver/carbon system was examined by the sessile drop method under vacuum at the temperature of 1243 K. Vitreous carbon, diamond and graphite were used as solid substrates. After wettability tests, the solidified Ag/C and Ag-X/C (X - 1 wt.% Ti or Zr) couples were subjected to structural characterization by SEM and EDX analysis. Liquid pure silver does not wet these substrates and shows weak adhesion, regardless of the type of the carbon material used. The introduction of 1 wt.% carbide forming additions Ti or Zr into silver changes dramatically the interaction in the Ag/C system leading to the formation of continuous reaction product layers (TiC_x and ZrC_x , respectively) at the drop/substrate interface. These interfacial layers are responsible for good wetting and high work of adhesion between AgTi1 and AgZr1 alloys and all types of carbon materials examined in this study.

Key words: wettability, adhesion, contact angle, Ag/C system

Wpływ Ti i Zr na zwilżalność i pracę adhezji w układzie Ag/C

Przedstawiono wyniki badań zwilżalności w układzie srebro/węgiel wykonanych w atmosferze próżni, w temperaturze 1243 K. Pomiary kąta zwilżania wykonano metodą leżącej kropli na podłożach z węgla szklanego, diamentu i grafitu. Po testach zwilżalności wytworzone pary materiałów Ag/C i Ag-X/C (X - 1% wag. Ti lub Zr) poddano analizie strukturalnej metodami SEM i EDX. Ag/C jest układem niereaktywnym, w którym srebro nie zwilża węgla. Prezentowane badania wykazują, że dodatek 1% wag. Ti lub Zr do srebra powoduje obniżenie kątów zwilżania i wzrost wartości pracy adhezji w układzie Ag/C niezależnie od typu materiału węglowego. Jest to związane z powstawaniem na granicy kontaktu kropli z podłożem węglowym warstw przejściowych zawierających węgliki TiC_x lub ZrC_x .

Słowa kluczowe: zwilżalność, adhezja, kąt zwilżania, układ Ag/C

1. Introduction

In many fields of material engineering the studies on new, innovative technologies depend on our knowledge of the phenomena occurring at the interface. The knowledge of interfacial phenomena related to adhesion and spreading kinetics is necessary for the fabrication of metal-ceramic composites and layered structures as well as in joining dissimilar materials [1 - 4].

From a practical point of view, in many technological applications it is particularly important to obtain a good adhesion between two solid phases. Such a good adhesion is commonly believed to be closely related to solid/liquid adhesion in the same system. In a design of a new technological process of material bonding it is absolutely crucial to determine adhesion energy in a liquid/solid system, even if bonding with a liquid phase is not predicted.

The Ag/C system belongs to the extensively investigated metal/ceramic systems because of its high importance for the synthesis of composite materials, e.g. Ag-C composites containing 2 - 5 wt.% C that are widely used as low-voltage electrical contacts. Due to their unique properties, such as excellent resistance to welding as well

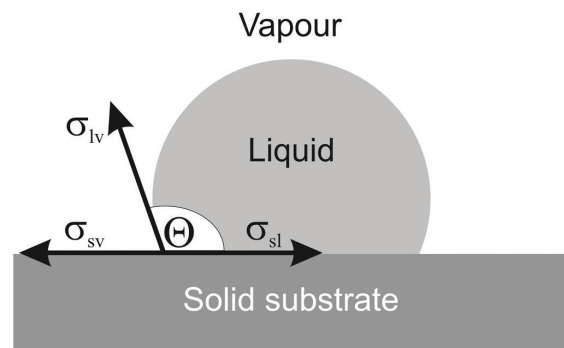


Fig. 1. Definition of the equilibrium contact angle θ : σ_{lv} – liquid/gas interfacial energy, σ_{sv} – solid/gas interfacial energy, σ_{sl} – solid/liquid interfacial energy.

Rys. 1. Równowagowy kąt zwilżania θ : σ_{lv} – energia powierzchniowa ciecz/gaz, σ_{sv} – energia powierzchniowa podłoże/gaz, σ_{sl} – energia powierzchniowa podłoże/ciecz.

as low and stable contact resistance, these composites are applied as contacts in current limiters (often used in asymmetric pairs), brush contacts, etc. [5]. Moreover, silver matrix composites containing carbon fibers offer highest thermal and electrical conductivity combined with

¹ Institute of Electronic Materials Technology, 133 Wólczyńska Str., 01-919 Warsaw, Poland, e-mail: Danuta.Grzybek@itme.edu.pl

² Center of High-Temperature Studies of Metals and Alloys, Foundry Research Institute, 73 Zakopiańska Str., 30-418 Cracow, Poland

low coefficient of thermal expansion. Therefore, they are promising candidates to be used in thermal management applications [6].

Silver and carbon do not react with each other and are mutually insoluble. Liquid silver does not wet carbon forming high contact angle $\theta \gg 90^\circ$ (Fig. 1) [7 - 9] and thus low work of adhesion (W_A) calculated from Young-Dupré equation [1 - 4]:

$$W_A = \sigma_{lv} (1 + \cos\theta), \quad (1)$$

where:

σ_{lv} – liquid/gas interfacial energy,
 θ – contact angle.

In non-reactive systems, such as Ag/C, van der Waals forces dominate at the liquid/solid interface. The value of these forces is directly proportional to the density of atoms on the contact surface and inversely proportional to their squared distance [6 - 9]. As a result, adhesion and wettability depend on atomic density on the contact surface and are related to crystallographic orientation of the substrate, which was confirmed experimentally and presented in Refs. [8 - 9]. Nogi et al. [9] studied the influence of substrate crystallographic orientation on wettability in non-reactive systems, like metal/C (diamond). In the case of diamond, the atomic density on the crystallographic planes decreases in the following order: (111)>(110)>(100). Among the metals that were the subject of studies (Bi, Pb, Sn, Ag, Au, Cu), the lowest contact angle and the highest work of adhesion were observed for the closest packed crystallographic plane of diamond, i.e. (111). The only exception was Ag, in the case of which the contact angle for the same plane was the highest of all planes, i.e. 147° , while the values for (110) and (100) planes were 103° and 135° , respectively. These measurements were carried out in hydrogen atmosphere at temperature 1273 K.

One way of improving the wettability and obtaining a good bonding in non-reactive metal/ceramic couples is to use an additive of an active element, exhibiting chemical affinity to the substrate. As a result, a non-reactive system can transform into a system, where interfacial chemical interactions are present. Ti, Zr, Cr and Si are often used as such active additives [10 - 13].

It should be highlighted that wettability in a metal/ceramic system is affected not only by its thermodynamic properties (mutual solubility, reactivity), but also by such external factors as: temperature and atmosphere of the process, impurities, surface roughness, crystallographic orientation, etc. [13 - 15].

2. Experimental procedure

The examination of wettability in the silver/carbon system was carried out using vitreous carbon (C_v), diamond (C_d) and graphite (C_g) as the substrates. The effect of active additives of Ti and Zr on the wetting behavior in the Ag/C system was studied. The wettability tests were performed for pure silver and silver alloys containing 1 wt.% of the active element, i.e. AgTi1 and AgZr1 alloys, respectively.

The contact angle was measured by the sessile drop method in which the images of a drop placed on a flat, smooth and leveled substrate were recorded vs time. A classic procedure of contact heating (CH) of a couple of examined materials was applied in the wettability tests. The measurements were carried out at the Center for High-Temperature Studies of the Foundry Research Institute in Cracow using high temperature facility described in details in Ref. [16].

Silver of high purity (99.999%) and the active additives of titanium (purity 99.99%) and zirconium (purity 99.95%) were used in the experiments. During the wettability tests silver alloys with the active additives were produced *in situ* directly in a vacuum chamber. Prior to placing the weighted metal portions into the vacuum chamber, their surfaces were cleaned ultrasonically in acetone and then in ethanol. A weighted portion of the reactive additive was slightly pressed into the silver sample and the whole assembly was placed onto the carbon substrate so that the additive remained at the top and did not have a contact with the substrate. During the heating, the process of melting the sample started from the top and ended at the time when a liquid drop was formed (Fig. 2).

Amorphous vitreous carbon, polycrystalline graphite and diamond obtained by CVD method were applied as substrates.

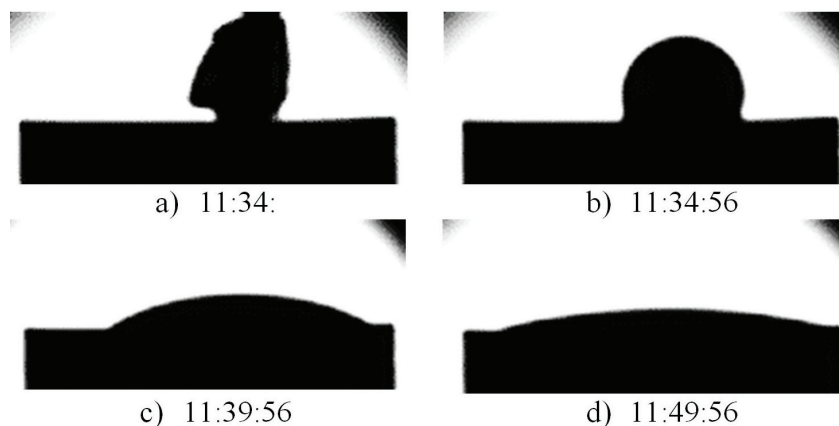


Fig. 2. Process of AgZr1 alloy drop formation: a) sample of weighted metals, b) a drop just after reaching the melting point, c) the drop after 5 minutes of heating, d) the drop after 15 minutes of heating.

Rys. 2. Proces formowania się kropli stopu AgZr1: a) naważka metali, b) kropla po osiągnięciu temperatury topnienia, c) kropla po 5 minutach wygrzewania, d) kropla po 15 minutach wygrzewania.

tes. Surface roughness (R_a), measured by an ALHA-STEP profilograph, was as follows: 6.5 nm for vitreous carbon, 4.5 nm for diamond and 30 nm for graphite (measuring length, $L_c = 400 \mu\text{m}$).

The wettability tests were carried out in ultra-high vacuum (5×10^{-3} Pa), at a temperature of 1243 K. After reaching this temperature, the samples were heated for 15 minutes and then cooled to RT. Both heating and cooling were performed at a rate of ~ 11 K/min. During the experiment, the drops were imaged by high-resolution digital camera at a rate of one frame per second. In order to calculate a contact angle θ , the collected images were analyzed using ASTRAView software, developed by CNR-Instituto per l'Energetica e le Interfasi – U.T. di Genova (Italy) [17 - 18]. After the wettability tests, the solidified couples Ag/C, AgTi1/C and AgZr1/C were subjected to structural characterization by scanning electron microscopy (SEM) and energy dispersive X-ray (EDX) analysis on the Zeiss Auriga SEM microscope. The cross-sections perpendicular to the surface of the substrate were investigated.

3. Results and discussion

The above experiments show clearly that the additive of 1 wt.% Ti or Zr improves wettability and increases adhesion in the Ag/C system, regardless of the kind of the substrate applied. The spreading kinetics of various forms of carbon by liquid silver and its alloys as well as the values of contact angles are presented in Figs. 3 and 4.

Just after melting the Ag sample on the vitreous carbon substrate, the contact angle θ was equal to 100° , and next after about 8 minutes it slightly increased to 106° , remaining practically constant during further heating of the Ag/C_v couple (Fig. 3a). A similar effect was observed in the Ag/C_d system with $\theta = 106^\circ$ (Fig. 3b), contrary to the Ag/C_g system in which θ was as high as 145° (Fig. 3c). These results represent experimental evidence of the effects of the allotropic form of carbon and substrate roughness on the value of contact angle in the Ag/C system.

In all the studied cases, the additive of 1 wt.% Ti or Zr to Ag caused a marked decrease in the contact angle. In the AgTi/C_v system, the value of θ_0 , formed immediately after the material melting, was 114° and then it was reduced to 87° in 146 s, followed by a systematic decrease up to the final value of $\theta_f = 26^\circ$ during further heating.

In the AgZr1/C_v system, the value of θ_0 was 171° and within 43 s the contact angle was reduced abruptly to 72° and finally reached $\theta_f = 13^\circ$.

It should be noted that due to the applied procedure of the *in situ* alloy preparation directly during the wettability tests, the initial values of contact angles (θ_0) represent the apparent values because at that time the drop of the alloy is still being formed and its shape often not ideal, especially

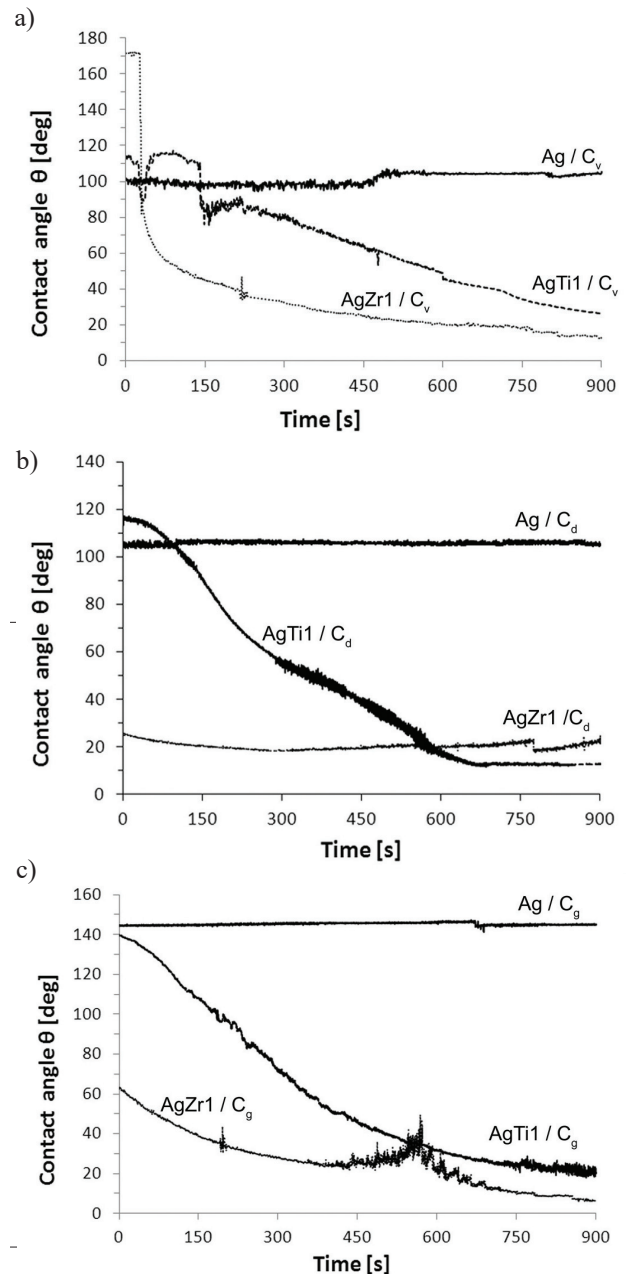


Fig. 3. Wettability kinetics in the Ag/C system (temperature: 1243 K, vacuum: 10^{-3} Pa) with different substrates: a) vitreous carbon – C_v, b) diamond – C_d, c) graphite – C_g.

Rys. 3. Kinetyka zwilżania w układzie Ag/C (temperatura: 1243 K, próżnia: 10^{-3} Pa), podłoże: a) węgiel szklisty - C_v, b) diament - C_d, c) grafit - C_g.

from the point of view of the required symmetry.

On the basis of the analysis of the curves representing the spreading kinetics it can be concluded that in the case of the non-reactive Ag/C system for all three studied substrates, the silver drop reached its equilibrium shape practically immediately after melting. Due to the additive of titanium or zirconium, the shape of the drop was varying during the whole period of the heating process. These observations are in line with the literature data,

which show that in non-reactive systems, the time of the drop spreading may be shorter than 1 s, in contrast to the reactive systems, where the spreading time can range from several seconds up to several hours [19 - 21], which is related to the formation of transition regions at the drop/substrate interface. Such layers can be formed due to a mutual solubility of components or they can result from the formation of the new phases as the products of a chemical reaction. After the crystallization of the liquid is terminated, the appearance of a solid/solid joint, can be observed, its nature depending on the kind of a system and the related type of liquid-solid interactions.

After wettability tests, metallographic specimens were subjected to EDX linear scan profiles of AgTi1/C and AgZr1/C interfaces (Figs. 5 - 8). In all these cases, the analysis of chemical composition revealed the formation of continuous reaction product layers. In the case of diamond

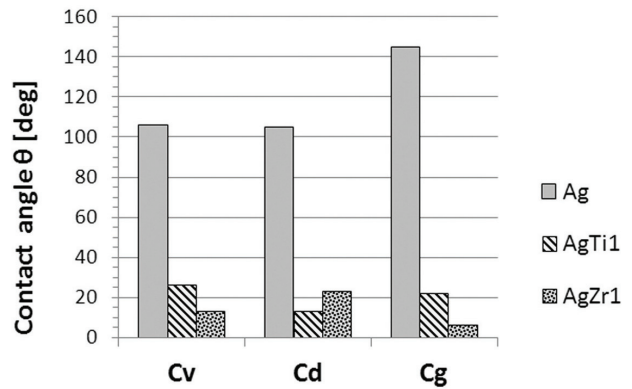
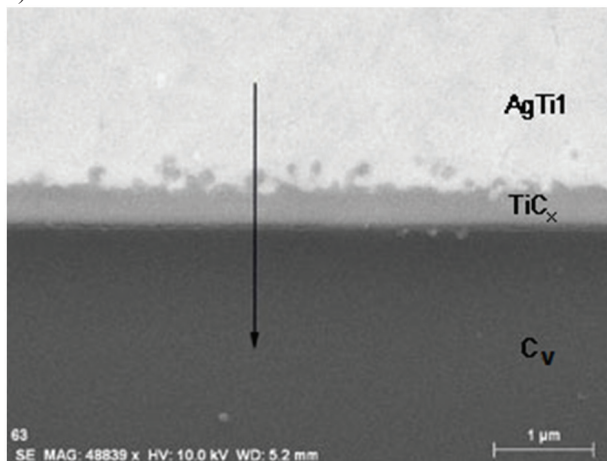


Fig. 4. Contact angles of pure Ag and its alloys AgTi1 and AgZr1 on investigated substrates (C_v – vitreous carbon, C_d – diamond, C_g – graphite).

Rys. 4. Kąty zwilżania na badanych podłożach (C_v – węgiel szklisty, C_d – diament, C_g – grafit).

a)



b)

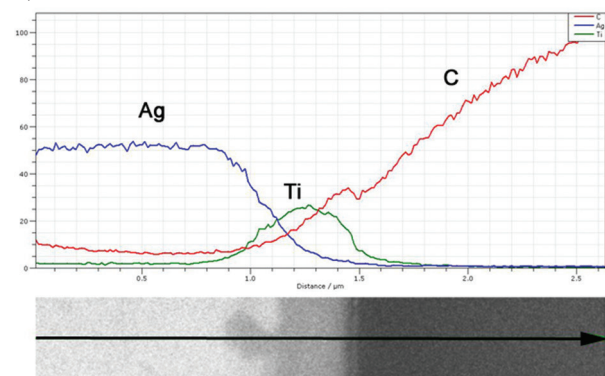


Fig. 5. SEM image of the AgTi1/ C_v interface (a) and compositional line analysis (b).

Rys. 5. Granica międzyfazowa AgTi1/ C_v (a) i rozkład liniowy zawartości pierwiastków (b).

a)



b)

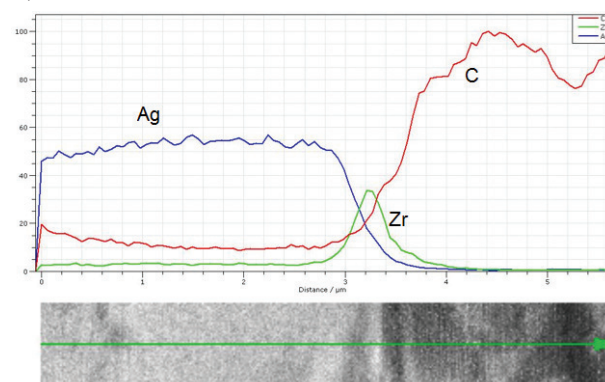


Fig. 6. SEM image of the AgZr1/ C_d interface (a) and compositional line analysis (b).

Rys. 6. Struktura granicy międzyfazowej AgZr1/ C_d (a) i rozkład liniowy zawartości pierwiastków (b).

substrates, the attempts to perform correct micro-sections failed. Nevertheless, it was observed that both titanium and zirconium additives have good interfacial bonding accompanied with an increased concentration of Ti or Zr and carbon within the interface region (Fig. 6), which suggests the existence of TiC_x or ZrC_x carbide.

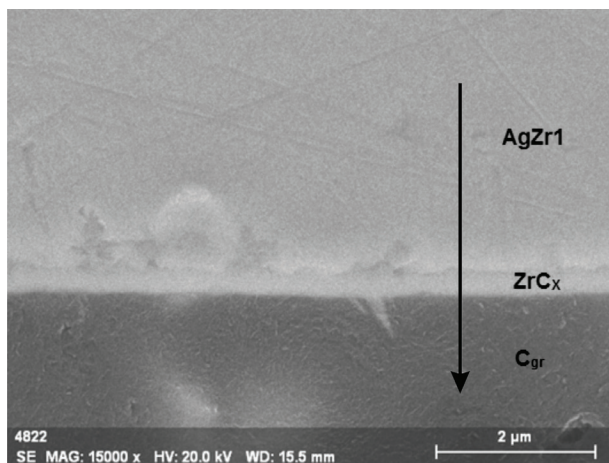
In the case of interaction between AgZr1 alloy with graphite substrate, the wetting, SEM and EDS analyses of the interfaces allowed us to identify not only the formation of intermediate regions of about 300 nm thickness (Figs. 7 - 8), but also the appearance of infiltration of the liquid alloy into the substrate open pores. Fig. 8 presents a high Zr concentration within the interface region and the impregnated zones.

SEM observations of the interfaces in AgTi1/C and AgZr1/C couples revealed the presence of transition regions of a thickness of about 300 nm (Fig. 5 - 8). According to the results of the linear scan profiles performed by EDX technique, AgTi1/C and AgZr1/C systems are characterized by the increased concentrations of carbon and reactive elements (Ti or Zr), which suggests the formation of carbides (Fig. 5 - 7). Following literature data

[22 - 23] it may be concluded that the forming transition regions can be composed of non-stoichiometric carbides (MeC_x type). In Refs. [22 - 23], Frage et al. investigated wettability in the Ag/TiC and Ag/ TiC_x systems in vacuum (10^{-3} Pa) at a temperature of 1323 K and demonstrated that liquid silver does not wet stoichiometric TiC forming the contact angle θ of 120° after 15 minutes. However, adding Ti additive to Ag significantly reduced the value of θ up to $30 - 35^\circ$ for 4 at.% Ti and 60° for 2.25 at.% Ti. Similarly, θ value decreases with a decrease in C content in TiC_x , namely from 120° for $x = 1$ to about 30° for $x = 0.55$.

Tab. 1 summarizes the values of the work of adhesion (W_A) calculated from the Young-Dupre equation (1). The values of the surface tension of pure Ag and its alloys AgTi1 and AgZr1 the same as those for pure silver (916 mJ/m^2 [24 - 27]) were used in the calculations. It was justified by the results of Novakovic et al. [28] who calculated the surface tension of pure Ag and Ag-Ti and Ag-Zr alloys by the QCA (Quasi Chemical Approximation) method. The negligible difference between these values at a temperature of 1473 K that is 230 K above the testing temperature of this study was also evidenced (Fig. 9).

a)



b)

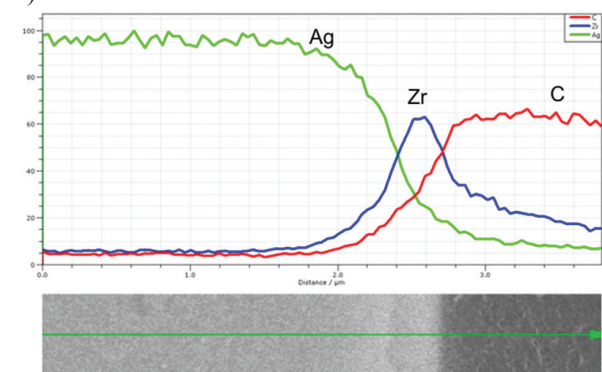
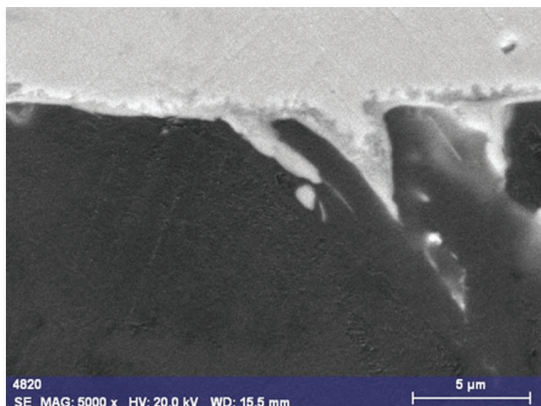
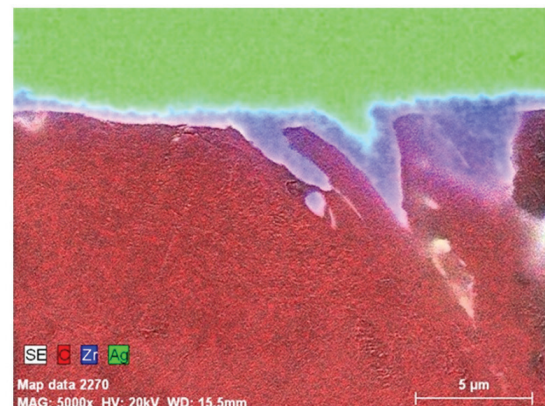


Fig. 7. SEM image of the AgZr1/C interface (a) and compositional line analysis (b).

Rys. 7. Granica międzyfazowa AgZr1/C_g (a) i rozkład liniowy zawartości pierwiastków (b).



a)



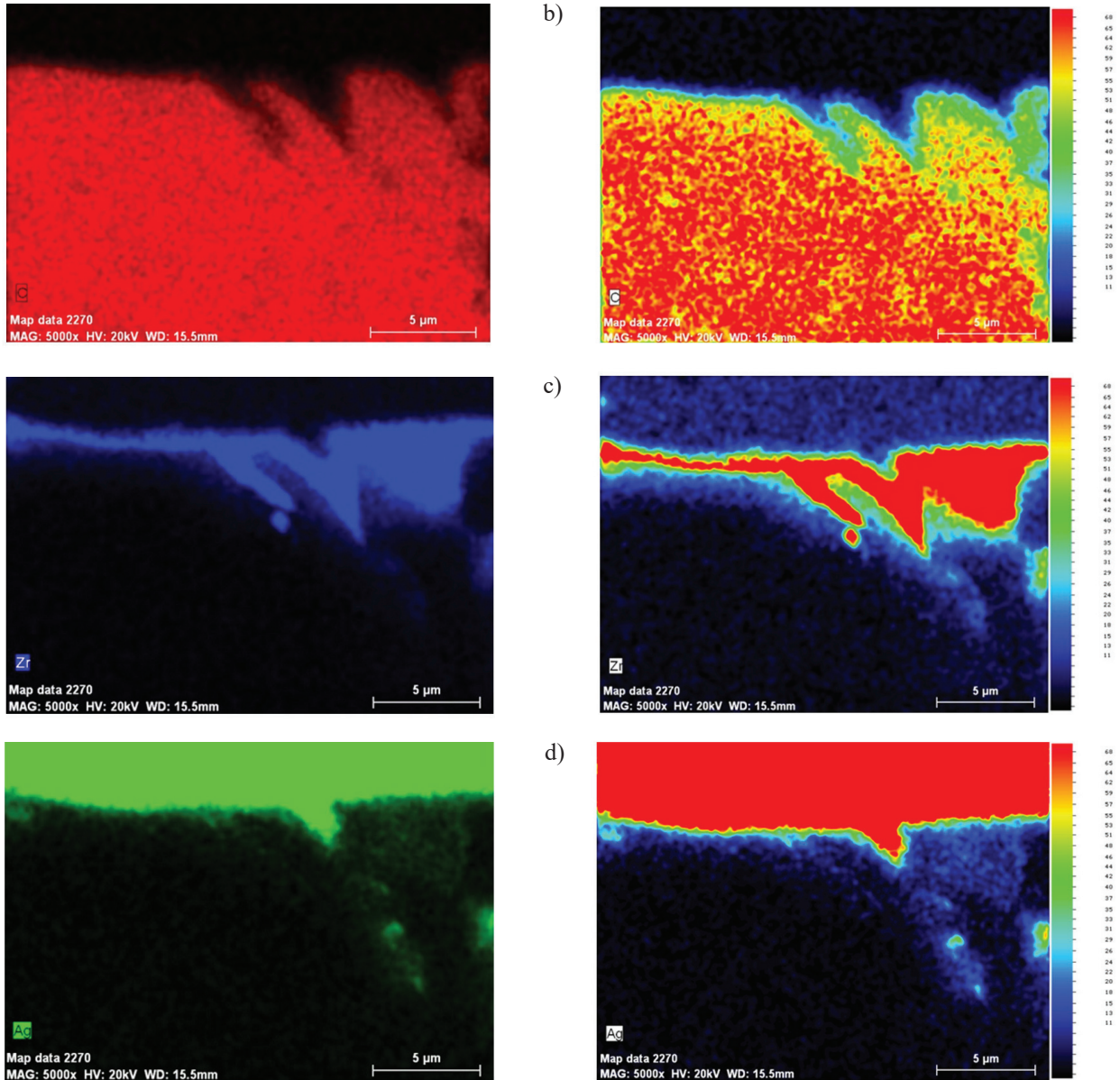


Fig. 8. SEM image of AgZr_1/C_g interface and surface distribution of C, Zr, Ag (a); surface distribution of elements (left hand side) and the corresponding intensity x-ray map (right hand side) of: C (b), Zr (c), Ag (d).

Rys. 8. Granica międzyfazowa AgZr_1/C_g i powierzchniowy zbiorczy rozkład pierwiastków C, Zr, Ag (a); powierzchniowy rozkład poszczególnych pierwiastków (strona lewa) i odpowiadająca im mapa intensywności sygnału rentgenowskiego (strona prawa): C (b), Zr (c), Ag (d).

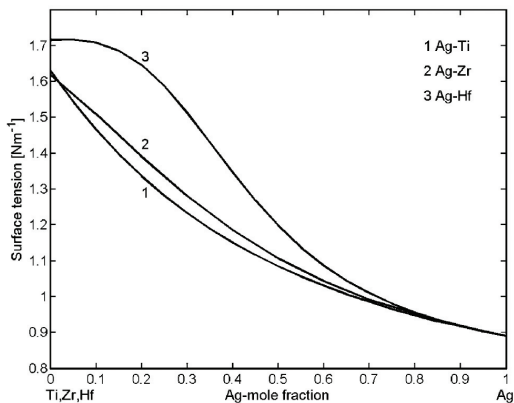


Fig. 9. Surface tension isotherms of liquid AgTi, AgZr and AgHf alloys calculated by the QCA method at $T = 1473 \text{ K}$ [28].

Rys. 9. Napięcia powierzchniowe ciekłych stopów AgTi, AgZr, AgHf, obliczone metodą QCA, dla temperatury 1473 K [28].

Tab. 1. The effects of alloying additions and the type of carbon material on the values of contact angle and work of adhesion in Ag/C system.**Tab. 1.** Wpływ dodatków stopowych oraz rodzaju materiału węglowego na wielkość kątów zwilżania i pracę adhezji w układzie Ag/C.

Substrate	Metal	Surface energy σ_{LV} [mJ/m ²]	Contact angle Θ [°]	Work of adhesion W_A [mJ/m ²]
Vitreous carbon	Ag	916	106	664
	AgTi1	916	26	1739
	AgZr1	916	13	1809
Diamond	Ag	916	105	679
	AgTi1	916	12	1812
	AgZr1	916	24	1753
Graphite	Ag	916	145	166
	AgTi1	916	21	1771
	AgZr1	916	6	1827

However, a decrease in the contact angle due to the addition of active elements in this study allowed to increase almost three times the work of adhesion in the Ag-alloy/C system, in comparison with that for pure silver.

4. Conclusions

Liquid pure silver does not wet examined carbon substrates and shows weak adhesion of the type of carbon material used. In contrast, the type of carbon material affects the value of the contact angle which at the temperature near the melting point of pure silver (1243 K) is for glassy carbon - about 106°, for the diamond - 105°, for graphite - 145°.

Introduction of a small amount (1 wt.%) of carbide forming Ti or Zr additions into silver results in a significant improvement of wettability. Depending on the type of carbon material, a reduction in the contact angle to 12 - 26° and up to 6 - 24° was found in the case of the AgTi1 and AgZr1 alloys respectively. Reactively formed interfacial layers (TiC_x and ZrC_x) are responsible for a significant improvement of wettability in the examined systems. This effect is accompanied with almost threefold increase in the work of adhesion, in comparison with that for pure silver.

Acknowledgement

The work was realized within a framework of a research project No. N N5103061 33 financed by the State Committee for Scientific Research of Poland.

References

- [1] Eustathopoulos N.: Wetting by liquid metals application in materials processing: The contribution of the Grenoble group, *Metals*, 2015, 5, 350 - 370, doi:10.3390/met5010350
- [2] Asthana R., Sobczak N.: Wettability in joining of advanced ceramics and composites: issues and challenges, *Ceramics Transactions*, 2014, 248, 589 - 600
- [3] Pereira J. C., Nascimento R. M., Martinelli A. E., Acchar W., Rocha L. A.: Wetting behavior of silver braze alloys onto metallized zirconia inserts, *Welding Journal*, 2015, 94, 211 - 217
- [4] Wu M., Cao C.-Z., Rafi-ud-din, He X.-B., Qu X.-H.: Brazing diamond/Cu composite to alumina using reactive Ag-Cu-Ti alloy, *Transactions of Nonferrous Metals Society of China*, 2013, 23, 1701 - 1708
- [5] Witter G. J.: Arcing contact materials. W: Electrical contacts Principles and applications, Marcel Dekker Inc. New York, 1999, ISBN:0-8247-1934-4
- [6] Hula R., Edtmaier C., Holzweber M., Hutter H., Eisenmenger-Sittner C.: The wetting behavior of silver on carbon, pure and carburized nickel, cobalt and molybdenum substrates, *Applied Surface Science*, 2010, 256, 4697 - 4701
- [7] Dezellus O., Eustathopoulos N.: The role of the van der Waals interactions on wetting and adhesion in metal/carbon systems, *Scripta Materialia*, 1999, 40, 1283 - 1288
- [8] Shen P., Fujii H., Nogi K.: Effect of substrate crystallographic orientation on wettability and adhesion in several representative systems, *Journal of Materials Processing and Technology*, 2004, 155 - 156, 1256 - 1260

- [9] Nogi K., Okada Y., Ogino K., Iwamoto N.: Wettability of diamond by liquid pure metals, *Materials Transactions, JIM*, 1994, 35, 3, 156 - 160
- [10] Dezellus O., Hodaj F., Mortensen A., Eustathopoulos N.: Diffusion-limited reactive wetting; spreading of Cu-Sn-Ti alloys on vitreous carbon, *Scripta Materialia*, 2001, 44, 2543 - 2549
- [11] Naidich Y.: About liquid metal/ceramic interface interaction mechanism and model of a new intermediate compound formation, *Current Opinion in Solid State and Materials Science*, 2005, 9, 161 - 166
- [12] Landry K., Kalogeropoulou S., Eustathopoulos N.: Wettability of carbon by aluminum and aluminum alloys, *Materials Science and Engineering A*, 1998, 254, 99 - 111
- [13] Sobczak N., Singh M., Asthana R.: High-temperature wettability measurements in metal/ceramic systems – some methodological issues, *Current Opinion in Solid State and Materials Science*, 2005, 9, 241 - 253
- [14] Eustathopoulos N., Sobczak N., Passerone A., Nogi K.: Measurement of contact angle and work of adhesion at high temperature, *Journal of Materials Science*, 2005, 40, 2271 - 2280
- [15] Kozlova O., Braccini M., Voytovych R., Eustathopoulos N., Martinetti P., Devismes M.-F.: Brazing copper to alumina using reactive CuAgTi alloys, *Acta Materialia*, 2010, 58, 125 - 1260
- [16] Sobczak N., Nowak R., Radziwill W., Budzioch J., Glenz A.: Experimental complex for investigations of high temperature capillarity phenomena, *Materials Science and Engineering A*, 2008, 495, 1, 43 - 49
- [17] Liggieri L., Passerone A.: An automatic technique for measuring the surface tension of liquid metals, *High Temperature Technology*, 1989, 7, 80 - 86
- [18] ASTRA Reference Book, IENI-CNR, Genova, Italy, Report, Oct. 2007
- [19] Landry K., Rado C., Voitovitch R., Eustathopoulos N.: Mechanism of reactive wetting: the question of triple line configuration, *Acta Metallurgica*, 1997, 45, 7, 3079 - 3085
- [20] Mortensen A., Drevet B., Eustathopoulos N.: Kinetics diffusion-limited spreading of sessile drops in reactive wetting, *Scripta Materialia*, 1997, 36, 6, 645 - 651
- [21] Eustathopoulos N.: Progress in understanding and modelling of reactive wetting of metals on ceramics, *Current Opinion in Solid State and Materials Science*, 2005, 9, 152 - 160
- [22] Frage N., Froumin N., Dariel M.P.: Wetting by non-reactive liquid metals, *Acta Materialia*, 2002, 50, 237 - 245
- [23] Frage N., Froumin N., Aizenstein M., Kutsenko L., Fuks D., Dariel M. P.: Reactive wetting in titanium carbide/non-reactive metal systems, *Current opinion in Solid State and Materials Science*, 2005, 9, 189 - 195
- [24] Missol W.: Energia powierzchni rozdziału faz w Metalach; Wyd. Śląsk, Katowice, 1975
- [25] Fima P., Sobczak N.: Thermophysical properties of Ag and Ag-Cu liquid alloys at 1098 K to 1573 K, *International Journal of Thermophysics*, 2010, 31, 1165-1174
- [26] Fathi Agra, Ahmed Ayyad: Surface energies of metals in both liquid and solid states, *Applied Surface Science*, 2011, 257, 6372 - 6379
- [27] Bernard G., Lupis H.P.: The surface tension of liquid silver alloys: part I. Silver-gold alloys, *Metallurgical Transactions*, 1971, 22, 555 - 559
- [28] Novakovic R., Tanaka T., Muolo M. L., Lee J., Passerone A.: Bulk and surface properties of liquid Ag X (X = Ti, Hf) compound forming alloys, *Surface Science*, 2005, 591, 56 - 69

The use of thermal mapping in evaluation of mechanically induced electrical degradation of graphene - based transparent heaters

Anna Kozłowska¹, Grzegorz Gawlik¹, Anna Piątkowska¹, Aleksandra Krajewska¹, Wawrzyniec Kaszub¹

The purpose of this study is to investigate temperature distributions of graphene-based transparent heaters deposited on glass. Furthermore it analyses the influence of layer discontinuities such as scratches and cracks on the performance of Joule-heated samples. Graphene mechanical strength was examined by the nanoscratch method at incremental loads using a ball on a flat sample surface. In the case of the controlled load several scratches were produced on the graphene surface. Tribological tests were conducted at different constant loads. The paper presents scanning electron micrograph (SEM) observations of the modified graphene surface. Infrared imaging of Joule-heated samples indicates a significant uniformity deterioration of the thermal maps due to the current flow alteration in the presence of structural imperfections. The results obtained in the course of this study give new insight into the role of defects such as cracks or discontinuities in the overall performance of graphene transparent layers.

Key words: graphene, transparent layer, heating element, infrared imaging, thermal distribution, mechanical defect



Zastosowanie mapowania termicznego do oceny elektrycznej degradacji uszkodzonych mechanicznie grafenowych przezroczystych elementów grzejnych

W pracy przeprowadzone zostały badania rozkładów termicznych elementów grzejnych zawierających warstwy grafenowe naniesione na szkło. Analizowany był wpływ nieciągłości warstwy w postaci zarysowań i pęknięć. Mechaniczna wytrzymałość grafenu badana była za pomocą metody nano-zarysowań przy narastającym obciążeniu kulki oddziaływującej na płaską powierzchnię próbki. Przy zastosowaniu kontrolowanego maksymalnego obciążenia wykonano szereg rys na powierzchni grafenu. Przeprowadzono testy tribologiczne dla różnych stałych obciążeń. W pracy zawarto wyniki analizy zmodyfikowanej powierzchni grafenu za pomocą skaningowego mikroskopu elektronowego (SEM). Obrazowanie w podczerwieni próbek podgrzewanych za pomocą wydzielanego ciepła Joula wskazały na znaczne pogorszenie jednorodności rozkładów termicznych, na skutek zmiany drogi przepływu prądu w przypadku występowania niedoskonałości strukturalnych. Wyniki pozwalają na ocenę wpływu defektów w postaci pęknięć i nieciągłości na działanie przezroczystych grafenowych warstw grzejnych.

Słowa kluczowe: grafen, warstwa przezroczysta, element grzejny, obrazowanie w podczerwieni, rozkład termiczny, defekt mechaniczny.

1. Introduction

Graphene attracts much interest because of its ability to conduct electric current of high density, almost uniform in the wide spectral range level of optical transparency, and because of its outstanding thermal properties. High optical transparency is particularly desirable for applications such as transparent screens, transparent Joule heaters integrated with glass windows [1 - 3], and photovoltaics or elastic displays [4]. Outstanding thermal properties such as high in-plane thermal conductivity make this material an ideal candidate for heat-spreading applications [5]. Structure variations (e.g. graphene wrinkles, grain boundaries), however, may introduce highly localized resistive heating and the rise of the temperature, both of which are likely to affect the reliability of graphene

devices [6]. Detrimental to the reliability is the presence of hot-spots, caused by the non-uniform current flow at the graphene layer discontinuities [7]. This effect leads to the accelerated degradation of the device, especially in the case of high current densities [8]. Although on a nanoscale, defect-free graphene is a robust material with an intrinsic strength reaching 42 N m^{-1} [9], in practical technical applications, a single-layer graphene is rather fragile and easily damaged. However, the role of the defects in the form of discontinuities and cracks in the modification of thermal performance of graphene-based transparent heaters was thoroughly investigated. In the paper, we describe the thermal behavior of a Joule-heated graphene sample with induced discontinuities. Graphene mechanical strength was examined by the nanoscratch method at incremental loads and tribological tests at different constant loads with the use of a ball tip. Mechanical defects introduced in this

¹ Institute of Electronic Materials Technology, 133 Wólczyńska Str., 01-919 Warsaw, Poland, e-mail: Anna.Kozłowska@itme.edu.pl

manner were analyzed using scanning electron microscopy (SEM). Joule-heating distributions of the modified graphene layers were examined using the high-resolution infrared imaging method.

2. Experimental

The graphene films were synthesized by chemical vapor deposition (CVD) on the surface of 35 μm thick copper foils. To obtain graphene on this material, we used the Aixtron Black Magic system with air-shower reactor. This kind of device ensures good stability and pyrometrically-controlled temperature and reasonable small thermal gradient effect. During the process we use pure (ultra high purity) hydrogen, argon and methane. In order to grow graphene on copper foil, the samples were heated up to 450°C (first step), 750°C and finally 960°C with presence of Argon and hydrogen. The growth of graphene was realized at 960°C and the methane flow with flow between 35 and 70 sccm during 12 minutes.

After the growth, the graphene on Cu foil was covered with a thin layer of poly (methyl-methacrylate) (PMMA) by a spin-coating method. This procedure prevents graphene film from destruction during the electrochemical delamination. A simplified scheme of this procedure is presented in the Fig. 1. After the electrochemical delamination, graphene with PMMA must be cleaned (RCA ceaning method) in deionized water and finally its covering dedicated substrate. Before removing PMMA, the samples were heated up to 120°C in a n air atmosphere. In the final step PMMA was removed into acetone and the sample was heated up once again up to 125°C. To characterize the graphene transferred onto the substrate, we performed

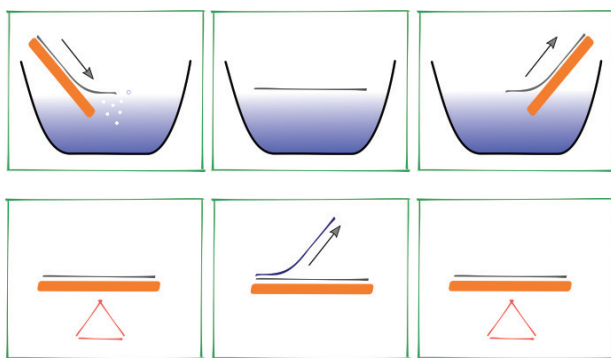


Fig. 1. Essential steps in the process of graphene transfer (from left to right): electrochemical delamination, cleaning process, covering graphene with PMMA on isolating surface, hot-plate, PMMA removing, hot plate.

Rys. 1. Podstawowe kroki w procesie przenoszenia grafenu (od strony lewej do prawej): delaminacja elektrochemiczna, proces czyszczenia, pokrywanie grafenu za pomocą PMMA, podgrzewanie, usuwanie PMMA, podgrzewanie.



Fig. 2. Photograph of graphene-based heater deposited on glass plate.

Rys. 2. Fotografia grzejnika grafenowego nałożonego na szklaną płytkę.

Raman spectroscopy as well SEM and AFM imaging. An Auriga cross beam workstation from Carl Zeiss was used for SEM characterization of the graphene surface.

Ohmic contacts to graphene were formed using silver conductive paste. A photograph of an exemplary graphene-based transparent heater is shown in Fig. 2. The size of the sample was 25 mm x 20 mm. The tribological system consisted of a ball on a flat surface with normal load of 0.8 N. The counterpiece was formed by a ceramic ZrO_2 ball with a diameter of 2 mm. The one-stroke mode was applied in tribological tests for a better observation of the graphene wear phenomena. Several graphene discontinuities could be observed on the graphene surface. The position of these scratches on the sample is schematically shown in Fig. 3a.

Infrared imaging was performed using the InSb 640 M camera (Thermosensorik / DCG Systems). A wide-field lens with the focal length of 28 mm was employed in this work. During the tests, the sample was placed on the heated table to register the calibration maps in the controlled temperature.

The course of the study was as follows: a pristine graphene sample was first examined using the infrared imaging (thermographic) method. In the next step, the tribological tests were made and the sample was observed under SEM and optical microscopes. Then, the sample was again characterized thermally using the infrared imaging method.

3. Results and discussion

The results of the thermographic characterization for a pristine, Joule-heated sample are presented in Fig. 3b-d. During the test, thermal maps were registered for the currents (I) ranging from 5.7 to 30.0 mA and the voltages (U) ranging from 10 to 50 V, resulting in the power surface density from 0.0114 W/cm² to 0.3 W/cm². An exemplary steady-state thermal map captured for $I = 30$ mA and $U = 50$ V is shown in Fig. 3b. It reveals the areas of elevated temperature located in the middle and the side part of the sample. In the upper part of the image, a distinct hot spot can be observed. Horizontal and vertical cross-sections through this hot spot for different supplied power levels are shown in Fig. 3c and Fig. 3d, respectively.

In the next step, as shown in the scheme in Fig. 3a, four scratches were made on the sample using the tribological system described in the previous section. SEM observa-

tions of the sample reveal different destruction mechanisms of the graphene layer depending on the applied load and on the adhesion of the graphene to the glass substrate. They are cohesive cracks, wrinkles formation under shear stress, delamination of the large graphene areas, destruction on folds, and tearing stripes, all of them leading to the formation of larger or smaller extended nonconductive areas, primarily in the form of scratches, which modify current flow in the graphene layer.

A SEM photograph of the tip of one of the scratches is presented in Fig. 4a. Apart from intentionally introduced cracks, observations of the sample indicate various defects such as the cracks, graphene discontinuities and wrinkles. Particularly, an ending point of a defect starting from the sample border can be observed at the position of the hot spot in the upper part of the sample (Fig. 4b). The sample with intentionally and accidentally introduced scratches was again characterized using the infrared imaging method. A thermal image captured for $U = 50$ V is shown

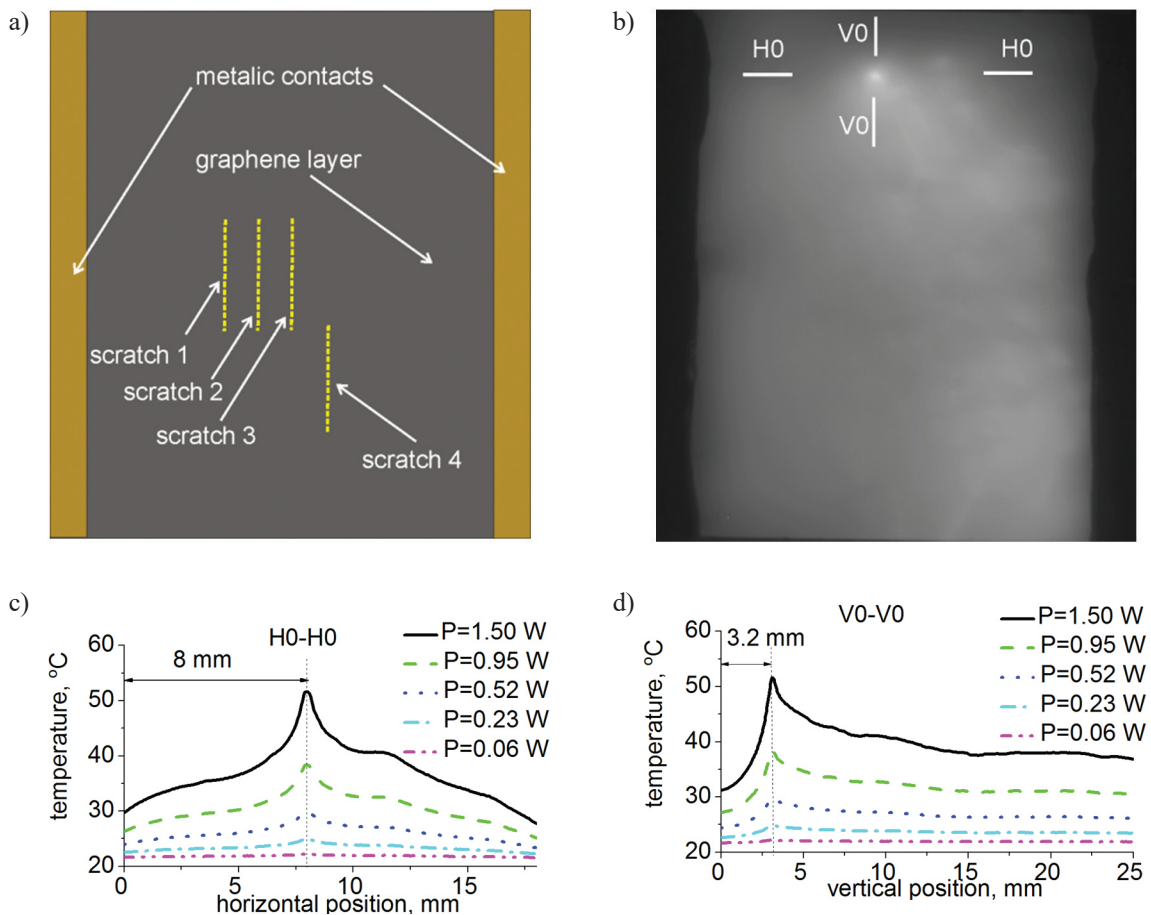


Fig. 3. Schematic of the sample and the results of the thermographic characterization of pristine CVD graphene sample. a) Drawing of the sample with the marked position of intentional scratches. b) Thermal image for a pristine sample biased with $I = 30$ mA and $U = 50$ V. c, d) Horizontal and vertical cross-sections through a hot spot for five supply power levels, respectively.

Rys. 3. Schemat próbki i wyniki charakteryzacji termograficznej 'wyjściowej' (niezmodyfikowanej) próbki z grafenem CVD. a) Rysunek próbki z zaznaczonym położeniem wykonanych rys. b) Obraz termiczny zasilonej próbki wyjściowej, $I = 30$ mA i $U = 50$ V. c, d) Odpowiednio: poziome i pionowe przekroje przez gorący punkt dla pięciu poziomów zasilania.

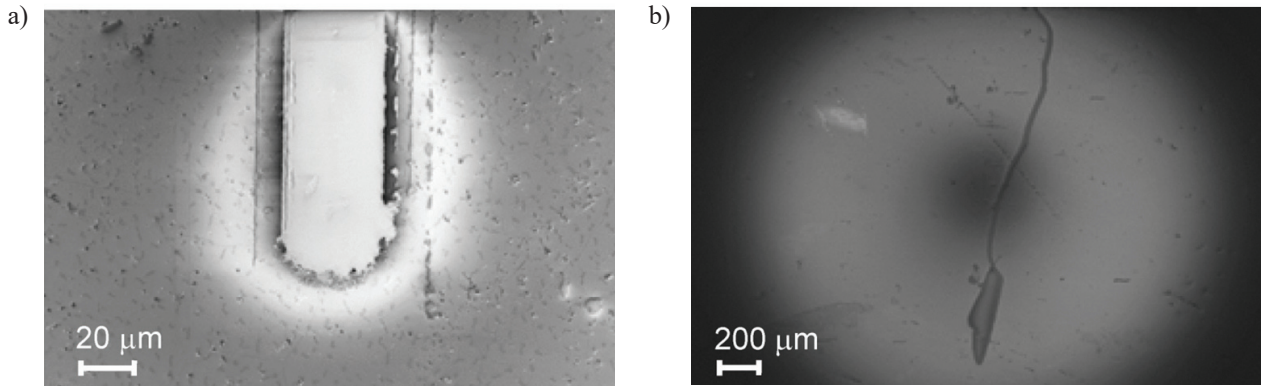


Fig. 4. SEM photographs of the graphene sample. a) Ending point of a scratch produced by nanoscratch method. b) Accidental defect on a graphene sample.

Rys. 4. Fotografia SEM próbki grafenowej. a) Końcowy fragment zarysowania wykonanego metodą nano-zarysowań. b) Przypadkowy defekt na próbce grafenowej.

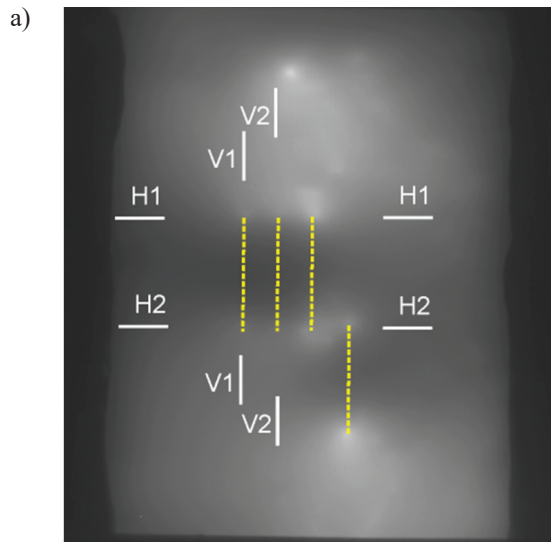
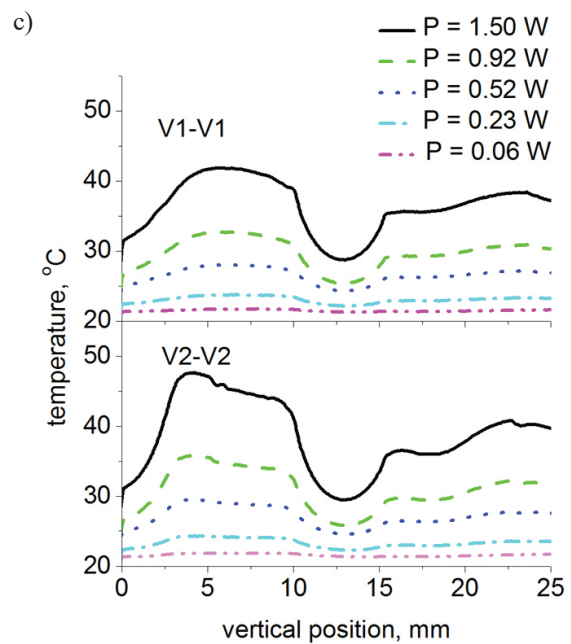
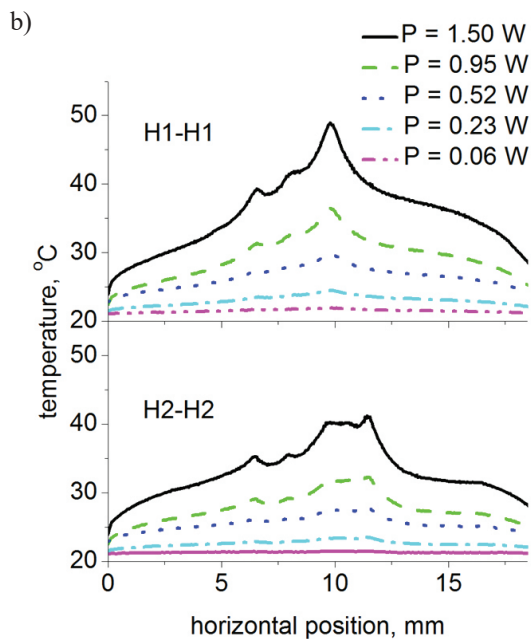


Fig. 5. Results of thermal characterization of graphene sample with intentionally introduced discontinuities. a) Thermal image for sample biased with $U = 50$ V (the position of scratches is marked with yellow dotted lines); b, c) horizontal and vertical cross-sections at marked positions, respectively.

Rys. 5. Wyniki charakteryzacji termograficznej próbki grafenowej z intencjonalnie wprowadzonymi nieciągłościami. a) Obraz termiczny zasilonej próbki, $U = 50$ V (położenie wykonanych rys zaznaczone jest żółtymi kropkowanymi liniami); b, c) odpowiednio: poziome i pionowe przekroje przez zaznaczone punkty.



in Fig. 5a. For clarity, the positions of the scratches are marked with the dotted lines.

Horizontal cross-sections at the marked position H1-H1 and H2-H2 for five power supply levels are shown in Fig. 5b. We can see local maxima at the positions of the scratch tips. In contrast, it becomes apparent that at the horizontal cross-section H2-H2, apart from local maxima that correspond to the starting points of scratches 1, 2, 3, and ending point of scratch 4, there is a smaller peak (at horizontal position 10.6 mm). Vertical cross-sections V1-V1 taken along scratch 1 (Fig. 5c) reveal the temperature decrease along at the scratched area and a small temperature increase at the scratch end. This effect can be observed at the cross-section V2-V2 taken along scratch 2. Here additionally, we can observe local maximum at the position 4 mm; this maximum is due to the hot spot in the upper part of the image.

To better evaluate the effect of mechanical defects on the thermal distributions, differential thermal images were calculated using thermographic camera software. These images illustrate how the thermal images of pristine sample changed due to mechanical modification of the sample. For this purpose, thermal images of pristine sample were inserted as reference images for the maps of the intentionally scratched sample (both reference and test maps were registered at the same bias level). An example of the resulting differential image for $U = 50$ V is shown in Fig. 6a. At horizontal cross-sections H1-H1 and H2-H2 (Fig. 6b), local maxima at the positions of scratch tips are clearly visible. In comparison, temperature decrease along the scratches is illustrated at vertical cross-sections V1-V1 and V2-V2 in Fig. 6c.

The results shown here clearly illustrate how alteration of current flow in a non-continuous resistive layer affects

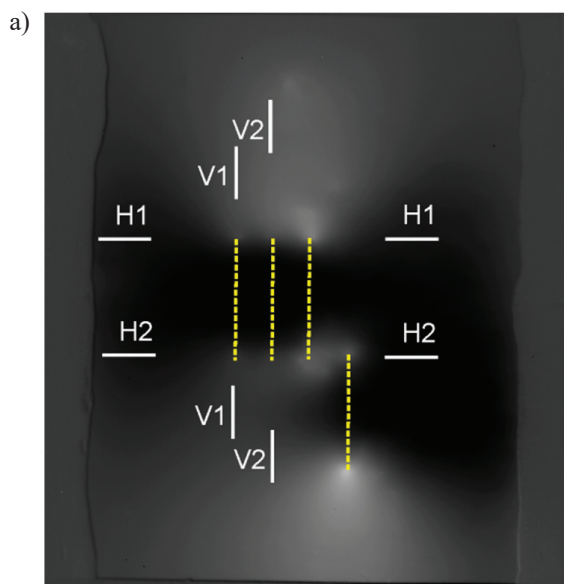
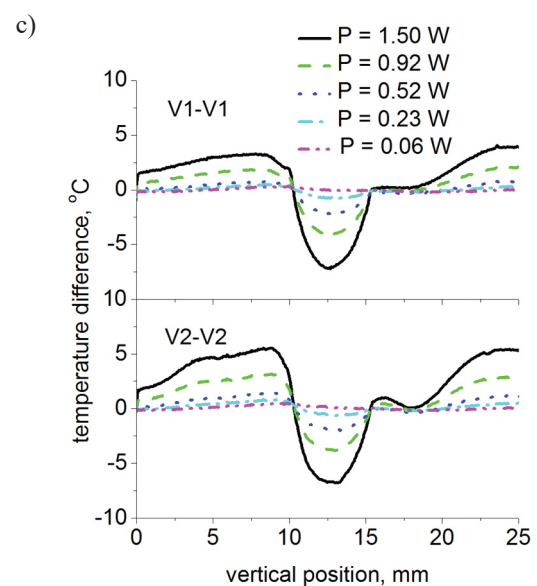
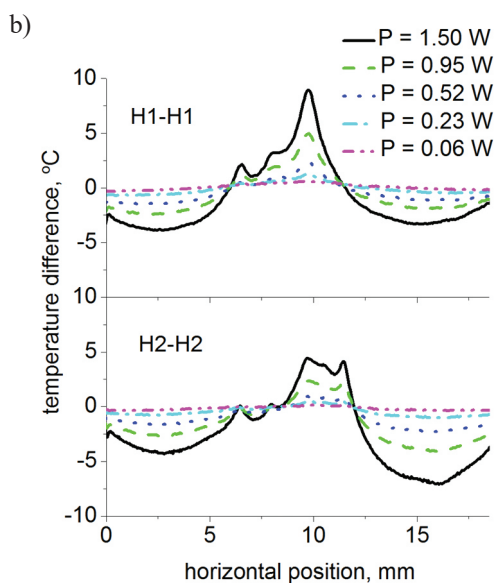


Fig. 6. Results of differential thermal measurements of graphene sample with intentionally introduced discontinuities. a) Differential thermal image for sample biased with $U = 50$ V (the position of scratches is marked with yellow dotted lines); b, c) horizontal and vertical cross-sections at marked positions, respectively.

Rys. 6. Wyniki różnicowych pomiarów termograficznych próbki grafenowej z intencjonalnie wprowadzonymi nieciągłościami.

a) Różnicowy obraz termiczny zasilonej próbki, $U = 50$ V (położenie wykonanych rys zaznaczone jest żółtymi kropkowanymi liniami); b i d) Odpowiednio: poziome i pionowe przekroje przez zaznaczone punkty.



the uniformity of the resulting thermal distributions. Typically, a crack starting from the border of the sample gives a Joule heating distribution in the form of a single hot spot, whereas rectangular defects result in two hot areas at the ends of the crack [7]. These effects can be observed in Fig. 3b, Fig. 5a, and 6a. A more complicated pattern is revealed at horizontal cross-sections H2-H2 shown in Fig. 3b and 4b, where an additional maximum can be observed. A microscopic observation shows that scratch 3, presented schematically in Fig. 3a as a straight line, in practical realization forms a small zig-zag at one end. Apart from the distinct hot-spots, thermal images show overall uniform deterioration, which is probably due to layer defects such as graphene wrinkles [6], which can be frequently observed in the SEM inspection.

4. Conclusions

Our study demonstrated the influence of the intentionally and accidentally introduced discontinuities on thermal distributions of Joule-heated CVD graphene deposited on a glass sample. Such non-conductive areas can be formed during the process of deposition of graphene or during the manipulation of the samples. In spite of the theoretically high fracture strength of graphene, our results indicate high fragility of a single-layer graphene. As the tribological tests show the application of even relatively small normal loads may be destructive for graphene when applied on a small contact area. Such structural imperfections give rise to locally higher electrical fields and high local temperatures. In practice, the presented results may provide a better understanding of the heat emissions from the graphene electrodes with complex shapes. Protective layers deposited on graphene might be a good solution in many practical applications of the heaters.

Acknowledgments

This work was supported by the Polish National Centre for Research and Development under the project no GRAF-TECH/NCBiR/06/30/2012.

References

- [1] Kang J., Kim H., Kim K. S., et al: High-performance graphene-based transparent flexible heaters, *Nano Letters*, 2011, 11, 12, 5154 - 5158, 10.1021/nl202311v
- [2] Kozłowska A., Kachniarz M., Gawlik G., Szewczyk R., Wojtasiak M.: Graphene Joule heating measurements in environmental chamber, *Progress in Automation, Robotics and Measuring Techniques, Advances in Intelligent Systems and Computing*, 2015, 352, 129 - 135
- [3] Wróblewski G., Kielbasiński K., Swatowska B., Jaglarz J., Marszałek K., Stapiński T., Jakubowska M.: Carbon nanomaterials dedicated to heating systems, *Circuit World*, 2015, 41, 3, 102 - 106, 10.1108/CW-05-2015-0021
- [4] Bonaccorso F., Sun Z., Hasan T., Ferrari A. C.: Graphene photonics and optoelectronics, *Nature Photonics*, 2010, 4, 611 - 622, 10.1038/nphoton.2010.186
- [5] Li X., Fang M., Wang W., Guo S., Liu W., Liu H., Wang X.: Graphene heat dissipation film for thermal management of hot spot in electronic device, *J. Mater. Sci.: Mater. Electron.*, 2016, 27, 7715 - 7721, 10.1007/s10854-016-4758-0
- [6] Grosse K. L., Dorgan V. E., Estrada D.: Direct observation of resistive heating at graphene wrinkles and grain boundaries, *Appl. Phys. Lett.*, 2014, 105, 143109 - 143112, 10.1063/1.4896676
- [7] Kozłowska A., Gawlik G., Szewczyk R., Piątkowska A., Krajewska A.: Infrared Thermal Emission from Joule-Heated Graphene with Defects, Asia Communications and Photonics Conference 2014, OSA Technical Digest, paper AT4B.2, 10.1364/ACPC.2014.AT4B.2
- [8] Beechem T. E., Shaffer R. A., Nogan J., Ohta T., Hamilton A. B., McDonald A. E., Howell S. W.: Self-heating and failure in scalable graphene devices, *Scientific Reports*, 2016, 6:26457,1 - 7
- [9] Lee C., Wei X., Kysar J. W., Hone J.: Measurement of the Elastic Properties and Intrinsic Strength of Monolayer Graphene, *Science*, 2008, 321, 385 - 388, 10.1126/science.1157996

Evaluation of hydrophobic properties of organic layers modified with graphene flakes

Beata Stańczyk¹, Krzysztof Góra¹, Katarzyna Jach¹, Lech Dobrzański²

The paper presents the results of our research on graphene composites with organic polymers in various media. The following composites have been tested: PVDF/DMF/GR, PVDF/NMP/GR, PVDF/acetone/toluene/GR and PMMA/GR. The main purpose of this study is to evaluate hydrophobic properties of the selected materials by the contact measurements angle using the static method. The highest obtained value of the contact angle approached 180° for a superhydrophobic composite PVDF/acetone/toluene/GR.

Key words: hydrophobic surface, contact angle, PMMA, PVDF, graphene



Ocena właściwości hydrofobowych pokryć organicznych modyfikowanych grafenem płatkowym

W artykule przedstawiono rezultaty prac dotyczących kompozytów grafenowych z polimerami organicznymi w różnych ośrodkach. Badano PVDF/DMF/GR, PVDF/NMP/GR, PVDF/acetone/toluene/GR i PMMA/GR. Główny przedmiot badań stanowiła ocena właściwości hydrofobowych wytypowanych materiałów. Weryfikowano je za pomocą pomiarów kąta zwilżania metodą statyczną. Najlepszymi parametrami charakteryzował się kompozyt PVDF/acetone/toluene/GR, który wykazywał właściwości superhydrofobowe z wartościami kąta zwilżania wodą zbliżonymi do 180°.

Słowa kluczowe: powierzchnia hydrofobowa, kąt zwilżania, PMMA, PVDF, grafen

1. Introduction

Wettability is defined as the ability of a liquid to maintain a contact with the surface of a solid. It is characterized by the contact angle (CA), whose value results from an equilibrium between the adhesion forces, which are of the surface origin, and the cohesion forces, i.e. the intermolecular interactions inside a drop of water. This state causes the appearance of the surface tension at the A/B interface. A low value of the surface tension indicates that cohesive forces (A-A and B-B types of cohesion) exceed the adhesion forces at the A/B interface. In this case the value of CA becomes very high and the surface of the solid is defined as hydrophobic.

Theories concerning superhydrophobic and superhydrophilic surfaces are currently being investigated by different groups of scientists representing such fields of science as material science, botany, physics and chemistry. The discovery of the lotus effect by Wilhelm Barthlott and Christoph Neinhuis initiated a rapid increase in the interest in these phenomena, although the relationship between the surface roughness and wettability had been already demonstrated in the 1940s by Cassie and Baxter [1 - 3]. Over the recent decades, due to the development of the technologies and methods, such as scanning electron microscopy, the investigations on biological surfaces revealed the existence of complex microstructures. The observation of the natural phenomena, and their combi-

nation with the possibilities offered by nanotechnology [4], have enabled the ways to obtain surfaces with the desired properties.

The functionalization consists in the chemical and physical treatment of a given material in order to make it applicable in various branches of industry, from the textile and aircraft industries to the armaments industry. The surfaces are modified towards the desired properties. For instance, the hydrophobic surfaces are obtained by combining the proper morphology in a micro- or nano-scale with the specific properties of polymers [5]. There is a demand for highly hydrophobic layers, which are the basis of the technologies relying on antistatic and nonadhesive phenomena, and using the self-cleaning and anti-pollution mechanisms. The hydrophobic layers can also be used for protection against the accumulation of ice crystals, e.g. on the surfaces of airplanes, highways or various types of building structures. The accumulation of water on the bearing surfaces and in the gaps or pores results in the change of aerodynamic properties, an increase in aerodynamic resistance, weight, and also in cracking and disintegration of the structures from the inside. In addition, these materials become useful in biomedical applications [6 - 9].

In 2013, Dong and Yao [10] reported in *Scientific Reports* on hydrophobic layers obtained from a composite: graphene - octadecylamine (ODA), characterized by the contact angle value of 152°. The authors also showed

¹ Institute of Electronic Materials Technology, 133 Wólczyńska Str., 01-919 Warsaw, Poland, e-mail: Beata.Stanczyk@itme.edu.pl

² Institute of Electron Technology, Al. Lotników 32/46, 02-668 Warsaw, Poland

the examples of other hydrophobic graphene composites utilizing such organic compounds as PVDF-HFP, i.e. polyvinylidene fluoride-co-hexafluoropropylene or MEH-PPV, i.e. poly[2-methoxy-5-(2-ethylhexyloxy)-1,4-phenylenevinylene]. The attention was also paid to the differences in the quality of the layers covering smooth surfaces and those with microstructures. The obtained values of contact angles were as high as 152° [10]. Rafiee et al. in the text entitled *Superhydrophobic to Superhydrophilic Wetting Control in Graphene Films* [11] described the material properties dependent on the type of the support. The properties of graphene flakes, suspended in water and acetone, and then transferred onto a substrate, varied from superhydrophilic to superhydrophobic, with the contact angle values (for wetting by water) ranging from 0° to 160° . The authors studied the mixture of water and acetone in various proportions, and determined an exact relationship between the composition of the support and the contact angle values. The higher got the water content in the mixture, the lower CA values and the stronger hydrophilic properties were observed.

The article entitled *Hydrophobicorganic layers on smooth and 3-dimensional developed surfaces* [9] presented the results which confirmed a very strong effect of the support on the parameters of the tested materials. The contact values angle for PVDF polymer (polyvinylidene fluoride) dispersed in various media, wetted by water, varied from 4° in an NMP solution (N-methylpyrrolidone), through 90° in DMF (dimethylformamide) to 133° in an acetone-toluene mixture. The authors explained that the significantly different CA values were related to the polarity and dipole moment of the solvents used. It was also noticed that covering the structured surfaces with layers enhanced the properties of a given material. The best parameters were exhibited by PVDF in the acetone/toluene medium, with the CA values reaching 133° on the smooth substrates and increasing up to 150° on the structured surfaces.

The use of graphene and the introduction of an additional heterogeneity is expected to reduce further the surface energies of the low-energy polymers and it allows obtaining materials with superhydrophobic properties.

On the basis of the previous studies on the organic polymers [9], the most optimal solutions selected for the modification were those with the use of graphene flakes. Besides the contact angle value, the composite ability to form a homogeneous layer both on smooth and structured substrates was the decisive parameter in qualifying a given material for further experiments. The obtained graphene composites were tested in a goniometer and the contact angles were determined by a sitting drop method, while the quality of the obtained samples was evaluated by optical microscopy. In order to verify the hydrophobic properties, the experimental results presented in this article were compared with the previously published data concerning the polymers not modified with graphene [9].

2. Experimental

2.1. Reagents used and method of their preparation

2.1.1. Samples of reduced graphene oxide (rGO)

Asbury graphite was subjected to the expansion process. Then it was oxidized using the Hummers method [12], in the medium of sulfuric acid, potassium nitrate and potassium permanganate. The obtained graphene oxide was purified during centrifugation, which was followed by the exfoliation using an ultrasonic probe. Next, the graphene oxide suspension was reduced by the additive of hydriodic acid and again purified by filtration. After sonication, a stable suspension in N-methylpyrrolidone was obtained from the prepared rGO.

2.1.2. Preparation of PVDF samples

2.1.2.A. PVDF/DMF/rGO (1BGR solution)

Solution 1 was prepared by dissolving 10 g of PVDF in 100ml of dimethylformamide and followed by sonication for 20 minutes. The homogeneous solution was then diluted in a voluminal ratio of 1:2 (r1: DMF = r1B). The solution denoted as 1B was used to prepare a composite with reduced graphene oxide flakes. The suspension of graphene in N-methyl-2-pyrrolidone was mixed with the polymer solution in a 1:1 voluminal ratio and again sonicated for 20 minutes (1BGR solution).

2.1.2.B. PVDF/NMP/rGO (2GR solution)

Solution 2 was prepared by mixing 2.5 g of PVDF with 50 ml of N-methylpyrrolidone and then holding it for 20 minutes in an ultrasonic bath. This solution was a basis for the preparation of a composite of a fluoropolymer and graphene, in NMP (solution 2: rGO / NMP = 1: 1 \leftrightarrow 2GR) as the support.

2.1.2.C. PVDF/acetone/toluene/rGO (4GR solution)

During the preparation of solution 4, acetone was mixed with toluene (5:3) and added to 2.5 g of PVDF. The homogeneous mixture was subjected to sonication for 20 minutes. After adding the additive of toluene,

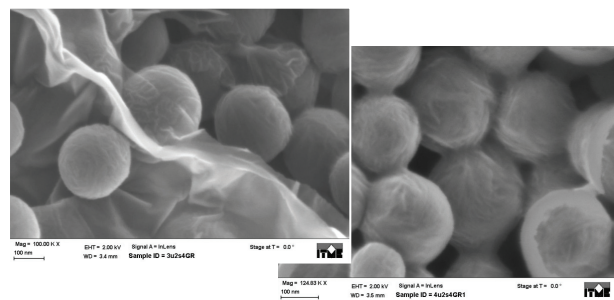


Fig.1. SEM image of the structure of a PVDF/acetone/toluene/GR composite.

Rys. 1. Obraz, z mikroskopu elektronowego, struktury kompozytu PVDF/aceton/toluen/GR.

the suspension of reduced graphene oxide in acetone was dispersed in solution 4, again by applying the ultrasonic for 20 minutes (solution 4: rGO/acetone/toluene = 1:1 ↔ 4GR). Fig. 1 shows the SEM images of the structure of a PVDF/acetone/toluene/rGO composite.

2.1.3. Preparation of the samples from PMMA/rGO (PMMAGR solution)

Graphene from the rGO/NMP solution was directly dispersed by sonication (20 minutes) in poly(methyl methacrylate) (PMMA) in a 1:1 voluminal ratio (PMMAGR).

2.2. Experimental methods

The process of covering the polymer layers modified with graphene was carried out directly on the four-inch silicon wafers (ITME) with (100) crystallographic orien-

tation. The desired geometry was obtained by photolithography, wet treatment and cryogenic plasma etching of silicon. The first step to obtain such profiles in the substrate was the deposition of SiO₂. Silicon oxide was prepared by a thermal oxidation of silicon wafers in PEO 603 furnace. Next, silicon oxide was etched with a NH₄F: HF: H₂O etching mixture, using the light sensitive emulsion as a mask. The obtained oxide was then used itself as a mask for plasma etching. The cryogenic process was carried out in the atmosphere of the mixed SF₆ and O₂ gases of 5N purity with the etch rate of ~ 1 μm/min. The produced structures were characterized by the following dimensions: 20/10 (m/d, closed structure); 10/20 (m/d, open structure); 15/5 (m/d); 10/10 μm (m/d) and a depth of ~ 10 μm (Fig. 2 and Fig. 3), where: "m" is the distance between the holes etched into the

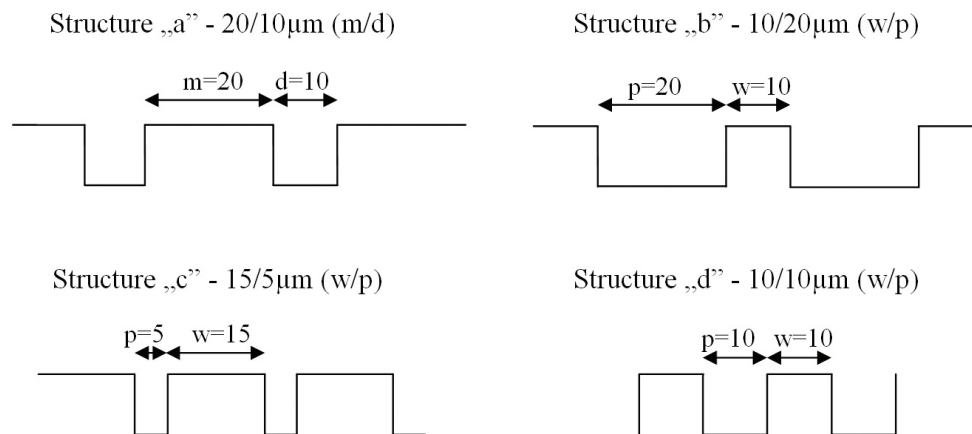


Fig. 2. Geometry of the structures obtained by cryogenic etching of silicon. „a” - 20/10 (m/d); „b” - 10/20 (w/p); „c” - 15/5 (w/p); „d” - 10/10 μm (w/p), where: "m" is the distance between the holes etched into the surface, "d" – the hole diameter; "w" - the side of the square of the hillock, "p" – the distance between the hillocks.

Rys. 2. Geometria struktur uzyskana w procesie kriogenicznego trawienia krzemu. „a” - 20/10 (m/d); „b” - 10/20 (w/p); „c” - 15/5 (w/p); „d” - 10/10 μm (w/p), gdzie: m/d - "m" oznacza odległość między otworami wytrawionymi w głąb powierzchni, a "d" średnica tego otworu; w/p - "w" to bok kwadratu wzgórek, a "p" przerwa - odległość między wzgórkami.

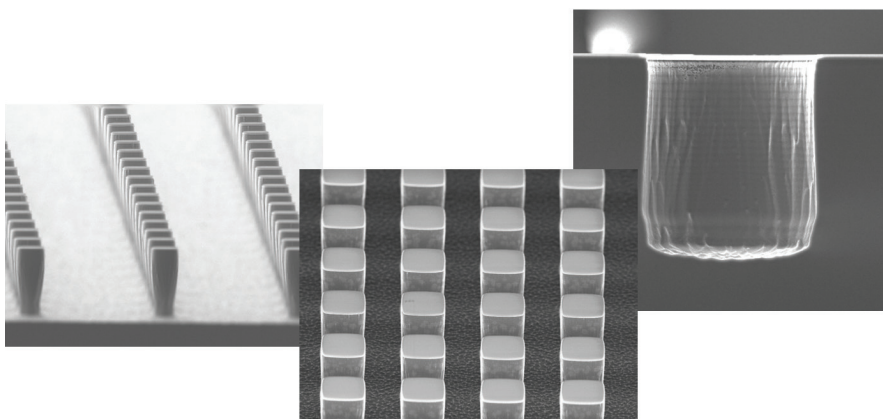


Fig. 3. Example SEM images of the structures which allow obtaining the lotus effect.

Rys. 3. Przykładowe zdjęcia SEM obrazujące struktury pozwalające na uzyskanie efektu „liścia lotosu”.

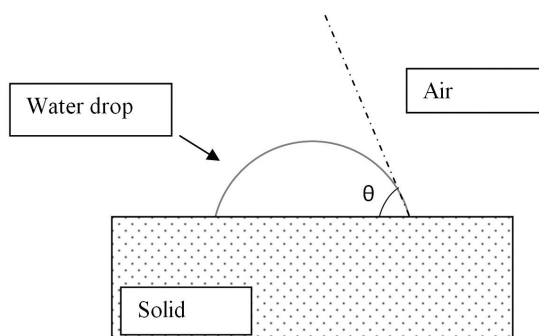


Fig. 4. The principle of the static method of the contact angle measurement.

Rys. 4. Zasada pomiaru kąta zwilżania metodą statyczną.

surface, "d" – the diameter of that hole; "w" - the side of the square of the hillock, "p" – the distance between the hillocks.

The composites were overlaid onto the smooth or structured silicon surfaces by sedimentation and centrifugation. Rotational speed and time varied from 400 to 3000 rpm and from 20 to 80 s, respectively. The substrates were prepared from poly(fluorovinylidene) - PVDF, $(-\text{CH}_2\text{CF}_2)_n$, $M_w = 534$, Sigma Aldrich, poly(methyl methacrylate) - PMMA (H5%), and modified with reduced graphene oxide flakes (ITME). Various compositions of solvents, such as N-methyl-pyrrolidone - NMP, acetone, toluene, N, N-dimethylformamide - DMF, were used.

2.3. Measurement of contact angle by static method

An optical goniometer coupled with a computer system served as the basic diagnostic tool that enabled the

contact angle measurements by the drop shape analysis after wetting the surface with water. The volume of a water drop dosed with a syringe was of the order of 5 μl . The principle of the contact angle measurement using the static method is shown in Fig. 4.

The contact angle ($\theta = \text{CA}$) is the angle between the tangent to the surface of the drop that is set on a solid at the point of a contact of three phases: solid, liquid and gas phase. The higher the contact values angle, the more hydrophobic are the properties of the material tested.

3. Results and discussion

The role of the additive of graphene to organic polymers has been verified by measuring the angle values contact. The graphene composites with PVDF/DMF, PVDF/NMP, PVDF acetone/toluene and PMMA have been tested.

The method of covering with layers was dependent on the properties of polymers [9], i.e. their viscosity. The images in Fig. 5 show the 1BGR samples with a PVDF/DMF solution as a support. This composite was overlaid onto a developed surface using two methods: centrifugation at low speed (Fig. 5a) and sedimentation (Fig. 5b). Only in the former case, the DMF-based composites, whose viscosity is of the order of 0.8 cP, lead to the silicon surface functionalization, giving homogeneous, smooth substrates. For the solutions characterized by the value of viscosity lower by a half, low-speed centrifugation does not guarantee a good quality of the substrate. In the latter case, the satisfactory layers are obtained by the deposition of the graphene composites by sedimentation (PVDF/acetone/toluene/rGO-solution 4GR).

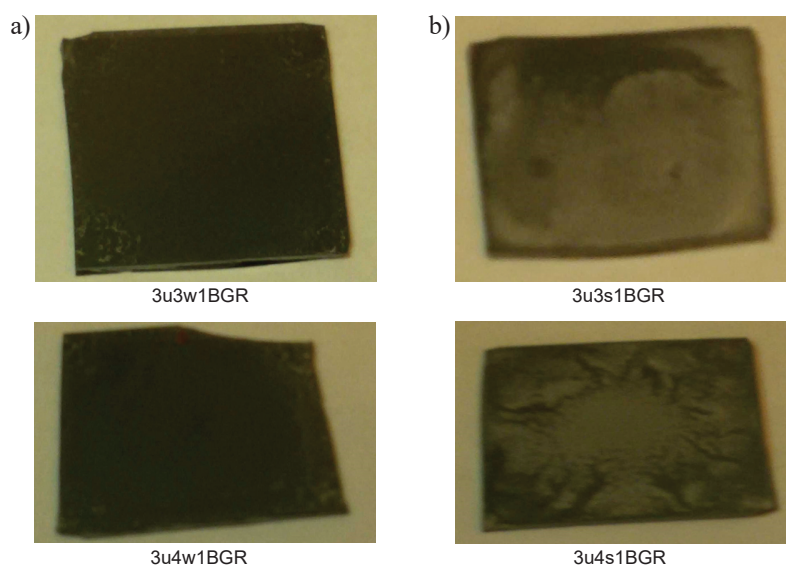


Fig. 5. Images showing the quality of the graphene/PVDF composite layers obtained by centrifugation (left pictures) and sedimentation (right pictures).

Rys. 5. Obrazy ilustrujące jakość uzyskiwanych warstw kompozytów polimerowo - grafenowych w zależności od metody nakładania: zdjęcia po lewej stronie a) wirowanie; zdjęcia po prawej stronie b) sedymentacja.

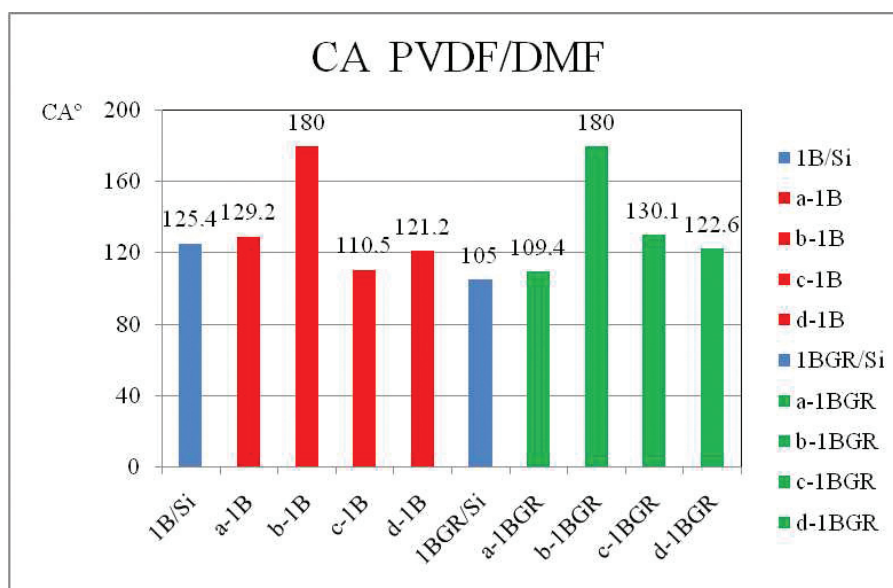


Fig. 6. The values of CA for PVDF/DMF and PVDF/DMF composites with graphene (1B i 1BGR solution) deposited by centrifugation on of the smooth (blue color) and developed silicon substrates (red color - 1B, green color – 1BGR): "a" - 20/10 (m/d); "b" - 10/20 (w/p); "c" - 15/5 (w/p); "d" - 10/10 μm (w/p), where: "m" is the distance between the holes etched into the surface, "d" – the hole diameter; "w" - the side of the square of the hillock, "p" – the distance between the hillocks.

Rys. 6. Wartości kąta zwilżania (CA) dla PVDF/DMF i kompozytów PVDF/DMF z grafenem (roztwór 1B i 1BGR) osadzanych metodą wirowania na podłożach krzemowych gładkich (kolor niebieski) i ze strukturami (kolor czerwony 1B, zielony 1BGR): "a" - 20/10 (m/d); "b" - 10/20 (w/p); "c" - 15/5 (w/p); "d" - 10/10 μm (w/p), gdzie: m/d - "m" oznacza odległość między otworami wytrawionymi w głąb powierzchni, a "d" średnica tego otworu; w/p - "w" to bok kwadratu wzgórek, a "p" przerwa - odległość między wzgórkami.

When applying this method, we can avoid the cleavage of the intermolecular bonds, which are weak in those solutions, and do not cause the formation of any unfavorable clusters or agglomerates on the surface.

Fig. 6 presents the contact angle values for wetting with water of PVDF dispersed in DMF (solution 1B-red color in Fig. 6) and its composite with graphene (1BGR solution - green color in Fig. 6), overlaid onto silicon. The analysis of this diagram shows that either the surface development (Figs. 6a, c, d) or the additive of rGO do not improve significantly the hydrophobic properties of the obtained surfaces. For both 1B and 1BGR polymers the average values of CA (calculated for the structure types: a, b, c, d) are $\sim 135^\circ$. Only for the structure b - 10/20 (w/p), the polymers and their composites cause the repulsion of the water drop and the values of CA reach 180° ($CA = 180^\circ$ is a limiting value, which is difficult to be determined and therefore conventionally assumed in this article).

Similar hydrophobic properties were observed for the material of graphene in PVDF/NMP/GR (2GR solution), obtained according to the procedure described in section 2.1.2.B. For this composite, the values contact angle were $\sim 130^\circ$, while the PVDF/NMP material not modified with graphene was characterized by strong hydrophilic properties.

The graphene composite in a PVDF medium, distributed in a mixture of acetone/toluene (4GR solution, according to section 2.1.2.C), exhibited a superhydrophobic character.

Fig. 7 shows a collection of the contact angle values for both the smooth and developed surfaces covered with the solution of PVDF polymer/acetone/toluene (taken from Ref. [9]) and its composite with graphene. The fact that the CA values equal to 180° for all surfaces with the additive of graphene composite, i.e. both the smooth and developed ones, demonstrates the unique properties of this material (blue and green color in Fig. 7). The comparison of the above parameters with those for a pure polymer confirms this hypothesis. The high CA values, ranging from $130 - 150^\circ$ for PVDF/acetone/toluene (red color in Fig. 7), reach the maximum values after the modification. The additive of graphene to a pure polymer enhances the hydrophobic effect of the obtained surfaces and causes a complete repulsion of the water drop.

Similar superhydrophobic properties were exhibited by a poly(methyl methacrylate)/graphene composite. The importance of the graphene additive to the polymer is demonstrated by the comparison of the average CA values for PMMA and PMMAGR, overlaid onto the smooth and developed surfaces (Fig. 8). These values are, respectively: 72° and 96° for the smooth surfaces (blue color in Fig. 8), and 134° and 165° for the developed surfaces (green color in Fig. 8). However, it should be noted here that the value 165° is an average of the following four individual CA values: 115.5° , 180° , 180° and 180° , obtained on four types of the structures, namely: a - 20/10 (m/d), b - 10/20 (w/p), c - 15/5 (w/p) and d - 10/10 μm (w/p). The analysis of these four CA values is consistent with

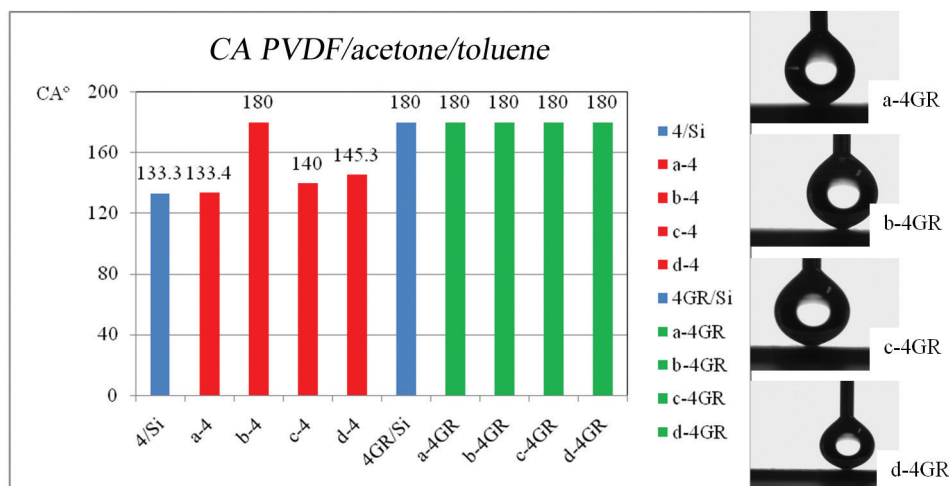


Fig. 7. The values of CA of PVDF/acetone/toluene (solution 4) and PVDF/acetone/toluene/GR, deposited by sedimentation on the silicon smooth (blue color) and structured substrates (red and green colors, respectively): "a" - 20/10 (m/d); "b" - 10/20 (w/p); "c" - 15/5 (w/p); "d" - 10/10 μm (w/p), where: "m" is the distance between the holes etched into the surface, "d" – the hole diameter; "w" - the side of the square of the hillock, "p" – the distance between the hillocks.

Rys. 7. Wartość kąta zwilżania (CA) dla PVDF/aceton/toluen (roztwór 4) oraz PVDF/aceton/toluen/GR osadzanych metodą sedymentacji na krzemowych podłożach gładkich (kolor niebieski) i ze strukturami (odpowiednio kolor czerwony i zielony): "a" - 20/10 (m/d); "b" - 10/20 (w/p); "c" - 15/5 (w/p); "d" - 10/10 μm (w/p), gdzie: m/d - "m" oznacza odległość między otworami wytrawionymi w głąb powierzchni, a "d" średnica tego otworu; w/p - "w" to bok kwadratu wzgórką, a "p" przerwa - odległość między wzgórkami.

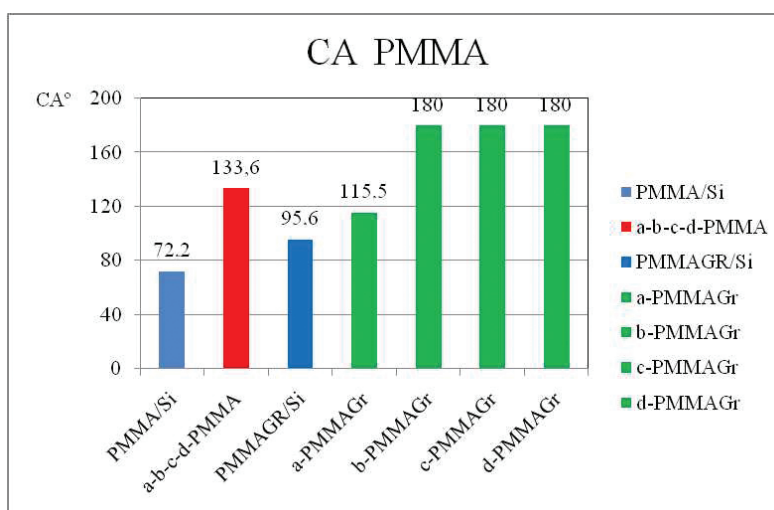


Fig. 8. The values of CA for PMMA (red color – an average calculated for the structures a, b, c, and d) and PMMAGR composites (green color) deposited by centrifugation of the smooth (blue color) and structured silicon substrates (red color - 1B, green color - 1BGR): "a" - 20/10 (m/d); "b" - 10/20 (w/p); "c" - 15/5 (w/p); "d" - 10/10 μm (w/p), where: "m" is the distance between the holes etched into the surface, "d" – the hole diameter; "w" - the side of the square of the hillock, "p" – the distance between the hillocks.

Rys. 8. Wartość kąta zwilżania (CA) dla kompozytów PMMA (kolor czerwony - średnia wartość obliczona dla struktur a,b,c,d) i PMMAGR (kolor zielony) osadzanych metodą wirowania na podłożach krzemowych gładkich (kolor niebieski) i ze strukturami: "a" - 20/10 (m/d); "b" - 10/20 (w/p); "c" - 15/5 (w/p); "d" - 10/10 μm (w/p), gdzie: m/d - "m" oznacza odległość między otworami wytrawionymi w głąb powierzchni, a "d" średnica tego otworu; w/p - "w" to bok kwadratu wzgórką, a "p" przerwa - odległość między wzgórkami.

the conclusions presented in the article *Hydrophobic organic layers on smooth and 3-dimensional developed surfaces* [9]. The closed structure of "a"-type does not guarantee an improvement in the hydrophobic properties and the adsorption on that surface proceeds similarly as on the smooth surface, which is illustrated in Fig. 8. For the smooth surface of PMMAGR/Si, the measured CA value

was 95.6°, while for the PMMAGR surface of "a"-type the values of CA reached 115.5°.

In most cases, the use of the reduced graphene oxide improved the hydrophobic properties of the prepared composites. Such behavior is due to the fact that the reduced graphene flakes are non-polar. The rGO flakes are free from oxygen atoms and the covalent bonds

between carbon atoms are unpolarised. They exhibit a strong affinity for the alkyl groups and combine easily with the hydrophobic PVDF polymer on various supports. The non-polar solvents additionally ensure a good dispersion of the flakes in the composite.

4. Conclusions

The article presents the results of the studies on graphene composites with organic polymers in various media. The following materials have been tested: PVDF/DMF/rGO, PVDF/NMP/rGO, PVDF/acetone/toluene/rGO and PMMA/rGO. The main subject of the research was the evaluation of the hydrophobic properties of the selected materials. These properties depend markedly on the medium, in which the material is dispersed, and on the way of coating the substrate with the material. The homogeneity of the composite layer was accepted as the evaluation criterion. The layers were deposited on the smooth and developed substrate surfaces. The composite of PVDF/acetone/toluene/rGO was characterized by the best parameters, i.e. by the contact angle value equal to 180° (superhydrophobic properties), for the material covering both smooth and structured surfaces. The CA value of 180° means that no adsorption of the water drop occurred on the composite during the measurement on the goniometer. This value did not depend on the type of the structure and was significantly greater than that obtained previously for a pure polymer. Graphene introduces an additional inhomogeneity and surface roughness, and combines well with the medium of PVDF/acetone/toluene, ensuring a good distribution of graphene film and a reproducibility of the deposition process. Because of the intermolecular interactions in the composite, the surface tension appearing at the interface is so small (the high values of CA are observed) that the water drop is repelled from the surface and superhydrophobic layer is formed.

References

- [1] Barthlott W., Neinhuis C.: Purity of the sacred lotus, or escape from contamination in biological surfaces, *Planta* 202, Springer, 1997, 1 - 8
- [2] Neinhuis C., Barthlott W.: Characterization and Distribution of Water-repellent, Self-cleaning Plant Surfaces, *Ann. Bot. (Oxford, U. K.)*, 1997, 79, 667 - 677
- [3] Wagner T., Neinhuis C., Barthlott W.: Wettability and Contaminability of Insect Wings as a Function of Their Surface Sculptures, *Acta Zool. (Stockholm)*, 1996, 77, 213 - 225
- [4] Koch K., Barthlott W.: Superhydrophobic and superhydrophilic plant surfaces: an inspiration for biomimetic materials, *The Royal Society*, 2009, 367, 1487 - 1509
- [5] Encyclopedia of Polymer Science and Technology, 2013, John Wiley & Sons B.
- [6] Li Y., Chen S., Wu M., Sun J.: All Spraying Processes for the Fabrication of Robust, Self-Healing, Superhydrophobic Coatings, *Adv. Mater.*, 2014, 26, 3344 - 3348
- [7] Falde E. J., Yohe S. T., Colson Y. L., Grinstaff M. W.: Superhydrophobic materials for biomedical applications, *Biomaterials*, 2016, 104, 87 - 103
- [8] Lim J. I., Kim S. I., Jung Y., Kim S. H.: Fabrication and Medical Applications of Lotus-leaf-like Structured Superhydrophobic Surface, *Polymer Korea*, 2013, 37, 4, 411 - 419
- [9] Stańczyk B., Dobrzański L., Góra K. et al.: Hydrophobicorganic layers on smooth and 3-dimensional developed surfaces, *Materiały Elektroniczne*, 2015, 73, 3, 25 - 34
- [10] Dong J., Yao Z., Yang T., Jiang L., Shen C.: Control of Superhydrophilic and Superhydrophobic Graphene Interface, *Scientific Reports*, 2013, 3, 1733, 1 - 6
- [11] Rafiee J., Rafiee M. A., Yu Z. Z., Koratka N.: Superhydrophobic to Superhydrophilic Wetting Control in Graphene Films, *Adv. Mater.*, 2010, 19, 22, 2151 - 2154
- [12] Hummers Jr. W. S., Offeman R. E.: Preparation of Graphitic Oxide, *J. Am. Chem. Soc.*, 1958, 80, 1339 - 1339